Received: 1 July 2025 | Revised: 17 February 2026 | Accepted: 24 February 2026

DOI: 10.1002/esp.70272

RESEARCH ARTICLE

ESPL WILEY

High-resolution LiDAR and stereo-DEMs for debris flow analysis in the Western Ghats, India: Sediment volume computation and run-out modeling

Krishnapriya V. K.[1] | Rajaneesh A.[1] | Sajinkumar K. S.[1,2] | Nikhil Nedumpallile-Vasu[3] | Yunus P. Ali[4] | Lina Hao[5] | Ajin R. S.[6] | Vanessa J. Banks[3] | Majdi Mansour[3] | Christian Arnhardt[3] | Binoj Kumar R. B.[1]

[1]Department of Geology, University of Kerala, Thiruvananthapuram, Kerala, India

[2]Department of Geological and Mining Engineering and Sciences, Michigan Technological University, Houghton, MI, USA

[3]British Geological Survey, Environmental Science Centre, Nottingham, UK

[4]Indian Institute of Science Education and Research, Mohali, Punjab, India

[5]College of Geography and Planning, Chengdu University of Technology, Chengdu, China

[6]Department of Earth Sciences, University of Florence, Florence, Italy

Correspondence
Sajinkumar K. S., Department of Geology, University of Kerala, Thiruvananthapuram, Kerala 695581, India.
Email: sajinks@keralauniversity.ac.in

Funding information
K.V.K.: The National Fellowship for Scheduled Caste Students (NFSC) of the Department of Social Justice and Empowerment, Government of India; NSFDC/E-81088. S.K.S. and Y.P.A.: Indian Space Research Organization- Disaster Management Support Programme (ISRO-DMSP) grant; ASCB/AS/2023/06. K.V.K., N.N.-V., V.J.B., M.M. and C.A.: BGS International NC Programme 'Geoscience to tackle Global Environment Challenges'; NE/X006255/1.

Abstract

Computation of sediment volume and accurate modeling of run-out using high-resolution digital elevation models (DEMs) are essential for assessing debris flow hazard. In this study, we used stereo-derived DEMs coupled with field observations and high-resolution LiDAR DEM to compute the depleted and accumulated sediment volume, and interpret the initiation phase of mobilized sediment from one of the catastrophic debris flows of the Western Ghats in India, the 1.2 km long Pettimudi debris flow of 2020 that killed over 70 people. Over 180 field-observed measurements were used to rectify the stereo-DEM, which was affected by dense vegetation. Accordingly, the depth of depletion over the scarp region was corrected from an overestimated value of ~25 m to a more accurate value of 7.08 m. The volume estimated using the DEM of Difference (DoD) of rectified DEMs shows that this debris flow progressively entrained and mobilized 17×10^4 m^3 of sediments. The Rapid Mass Movement Simulation (RAMMS) tool was used to simulate flow characteristics under conditions similar to those in the field. The high-resolution LiDAR DEM enabled us to validate debris flow simulations and provided an unprecedented record of their development and evolution at sub-second time resolution.

KEYWORDS
debris flow, DEM rectification, Pettimudi, Rapid Mass Movement Simulation (RAMMS), the Western Ghats

1 | INTRODUCTION

Debris flow is one of the most common and deadliest natural hazards in the mountainous regions (Korup & Clague, 2009; Larsen & Torres-Sánchez, 1998; Svalova et al., 2019), especially in the monsoon-prevalent tropical regions (Aristizábal et al., 2017; Nagarajan et al., 2000; Sajinkumar & Anbazhagan, 2015; Sim et al., 2022). Debris flows typically form along steep thalwegs, resulting in long run-out paths and devastating impacts in downstream areas due to their high velocity (dos Santos Corrêa et al., 2024; Veloso et al., 2023). Identifying the sources and quantifying the volumes of sediment contributing to debris flow development is crucial for understanding its dynamics (e.g., Morell et al., 2021; Tucker & Hancock, 2010). Run-out modeling for debris flows using such accurate input data will help with hazard assessment and the development of mitigation strategies.

Debris flows often are confined to lower-order basins (Allen & Hovius, 1998; Chowdhury, 2024; Ng, 2006), such as the colluvial parts of drainage channels or the first-order basins. Colluvial channels govern the movement of water and sediment from hill slopes to the fluvial network (Grieve et al., 2018), and first-order stream basins

include uppermost drainage network channels. During heavy rainfall, runoff-generated debris flows tend to travel long distances through lower-order streams, descending from elevated areas to the base of the slope, and eventually merging with the higher-order streams (Guinau et al., 2007). In most cases, a high drainage density and a concave slope with high stream power are characteristic features of such debris flows (e.g., Yang et al., 2020; Yunus et al., 2021). One such mountainous region is the Western Ghats in India, where this passive elevated continental margin facilitates orographic lifting of monsoon winds, resulting in heavy rainfall and numerous catastrophic landslides (Mathew et al., 2021; Sharma et al., 2022; Yesubabu et al., 2024). The high stream power and steep slopes over this mountain system facilitate the movement of shallow slide/flow-type landslides during extreme rainfall events (Ajin et al., 2022; Krishnapriya et al., 2024, Krishnapriya, Amrutha, et al., 2025, Krishnapriya, Rajaneesh, et al., 2025; Yunus et al., 2021; Yunus, Ishan, et al. 2025). During such events, debris flows can rapidly increase in volume through entrainment of slope materials along gullies and drainage channels, with sediment transport closely linked to runoff intensity and channel gradient (cf. Fusco et al., 2024; Radice et al., 2016; Rickenmann & Koschni, 2010). Such large-scale events can significantly influence the geometry of drainage divides, resulting in the reconfiguration of river basins and landscape transformation (cf. Dahlquist et al., 2018).

In debris flow susceptibility assessments, one often-overlooked aspect is the potential for run-out paths to extend into areas classified as low-susceptibility (Rajaneesh et al., 2025). This happens because the focus is often on where the debris flow initiates, without considering how far the debris might travel. Thus, the generated maps should encompass not only the areas where it may initiate, but also regions that could be impacted by the movement of mobilized material (Melo & Zêzere, 2017; Pareek et al., 2024). Therefore, modeling debris flow run-out in these regions, particularly in highly susceptible areas, is crucial for identifying zones prone to severe impact. To accomplish this, simulating possible debris flow run-out paths using high-resolution DEMs is crucial, especially for estimating sediment volume and assessing flow paths.

Utilizing high-resolution DEMs (e.g., 1 m or less), one can derive the drainage networks and associated catchments for debris flow studies, cross and long profiles, and source area volume depletion, as they offer precise topographical data that aids in recognizing and assessing slope characteristics and elevation variations (cf. Boreggio et al., 2022). Such detailed topographical information is essential for evaluating the extent of an area's susceptibility to debris flows and for modeling potential flow paths within the drainage basins. Moreover, identifying terrain features that influence flow initiation and routing, such as slope angle, aspect, curvature, and relief, will contribute to the development of more accurate susceptibility maps, which in turn can support early warning systems and mitigation strategies. Furthermore, the precision of run-out models also relies on the accuracy of the DEM, as inaccuracies can lead to errors in watershed delineation and flow routing (Degetto et al., 2015). A high-resolution DEM enhances simulation accuracy, as demonstrated by Michalsen (2018), particularly in replicating the shape, run-out, flow height, and velocity of a landslide at a site-specific scale. The pre-event DEM resolution, which emphasizes natural terrain surface geometry, is a crucial input parameter for modeling (Krušić et al., 2019). Furthermore, such DEMs facilitate volumetric analysis of landslides through pre- and post-event comparisons, enabling identification of affected areas and quantification of landslide volumes, which are essential for post-disaster management efforts (Atefi & Miura, 2021). High-resolution DEMs generated from non-invasive laser-scanning techniques have been used in several other geological studies, including the extraction of structural features and slope discontinuities, which are important for identifying potential failure surfaces relevant to debris flow initiation (Longoni et al., 2012; Roncella & Forlani, 2005). Although LiDAR-derived DEMs generally provide higher accuracy, their spatial and temporal availability is still limited in many densely forested tropical regions, particularly for pre-event terrain conditions.

Here, we use 1 m stereo-DEMs of pre-and post-event, and post-event LiDAR measurements at a sub-meter scale to measure volumes and spatial patterns of debris flow scour and deposition in the 2020 debris flow event at Pettimudi, the Western Ghats, India, that resulted in a 1.2 km run-out path with an initiation zone area of 7,399.23 m^2 and a deposition zone area of 10,074.6 m^2. This landslide catastrophically killed over 70 people. We coupled the DEM data with field observations to investigate the channel geometry and material characteristics of the entrainment phase and deposition zones. In tropical regions, airborne LiDAR acquisition can also be constrained by regulatory restrictions, logistical challenges, cost, and limited historical coverage, whereas stereo-DEMs offer long-term, global, and repeat coverage, making them one of the few viable options for retrospective pre-event analysis. Due to dense vegetation in tropical regions, stereo-DEMs produced by photogrammetric methods may contain inaccuracies, which will affect the overall simulation inputs. To address this, we outline a comprehensive approach to improve the accuracy of optically derived stereo-DEMs. This novel approach is intended as a complementary solution to LiDAR, providing a practical alternative when LiDAR data cannot be obtained due to technical, regulatory, temporal, or financial constraints. Such improvements are important for debris flow studies. Several studies have explored diverse DEM rectification approaches, focusing on improving accuracy through computational, photogrammetric, and statistical methods. Early works demonstrated digital image rectification and geometric correction using differential and polynomial models (Konecny, 1979; Lee & Han, 2020; Novak, 1992), while others examined the influence of ground control points (GCPs) and DEM accuracy on orthoimage precision (Dai et al., 2023,b; Jiao et al., 2008). Studies such as Wackrow & Chandler (2011) and James & Robson (2014) improved photogrammetric accuracy through optimized network geometry and self-calibration, whereas Mohamed (2008) and Zhao et al. (2015) applied statistical and interpolation-based rectification methods to refine photogrammetric and satellite DEMs, respectively. More recent research optimized unmanned aerial vehicle (UAV)—the structure from motion (SfM) acquisition strategies and flight parameters to reduce systematic deformation (Ait-Lamallam et al., 2025; Ouédraogo et al., 2014; Wang et al., 2025). To emphasize the conceptual distinction from earlier research, previous DEM rectification studies were reviewed and analyzed (Supporting Information S1), revealing that none have addressed the challenges of dense tropical canopy and steep terrain correction using a multi-sensor validation framework. While the above-mentioned approaches focus on improving DEM accuracy through computational techniques, acquisition strategies, and control data refinement across open, engineered, or sparsely

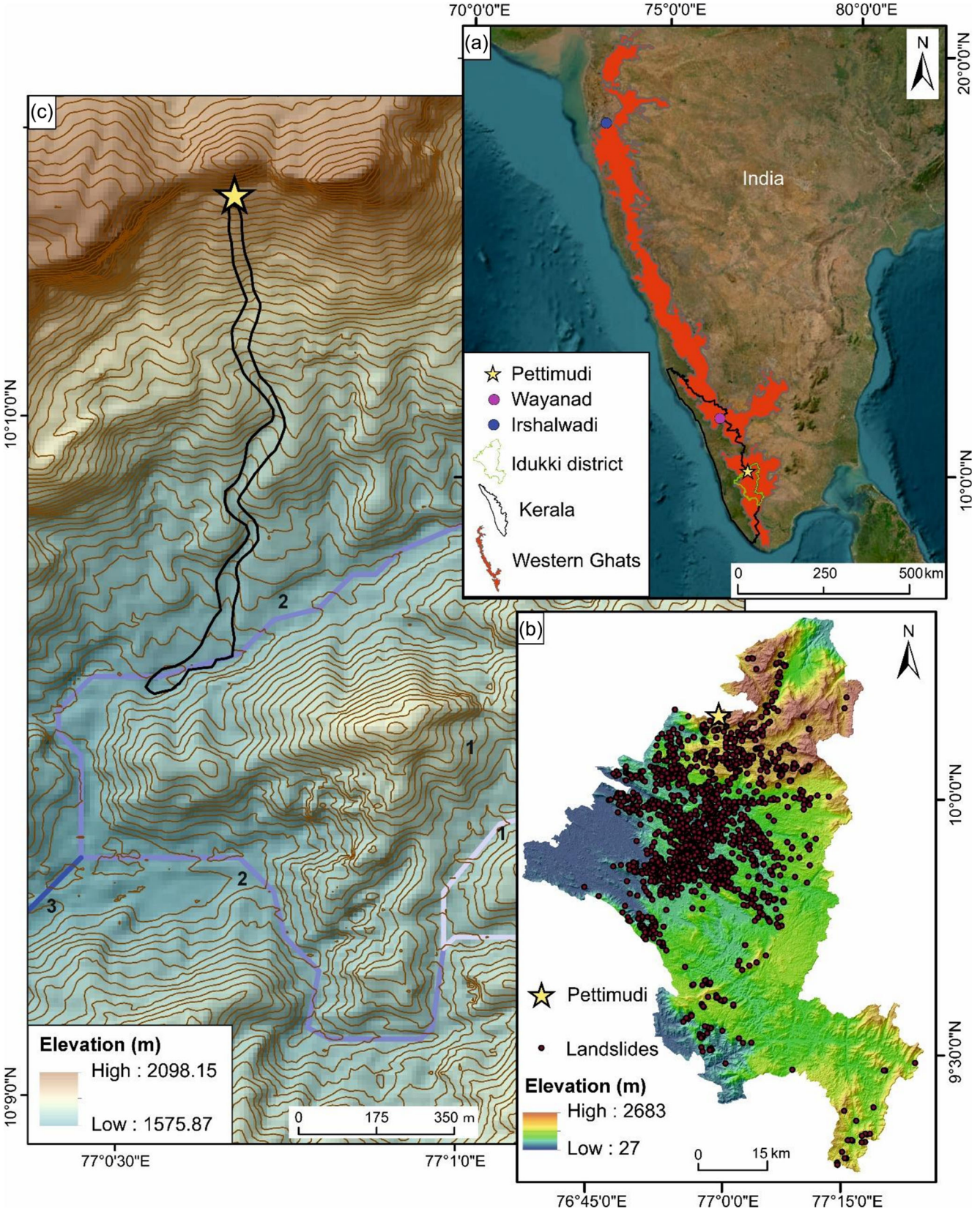

FIGURE 1 Location map of the study area **(a)** map showing the Western Ghats and the state of Kerala in India (Source: ArcGIS online basemap (ESRI, Vantor, Earthstar Geographics, and the GIS user community)) **(b)** elevation map of Idukki district with landslides of 2018 and Pettimudi landslide location **(c)** footprint of the Pettimudi landslide within the contour map (Source of 1b–c: Shuttle Radar Topography Mission (SRTM) elevation data).

vegetated terrains, our study introduces a novel field-validated methodology for rectifying stereo-DEMs in dense tropical mountain environments, addressing canopy interference and geomorphologically meaningful elevation correction for debrisflow modeling. We used over 180 physically measured field observations, a ground-truth-based approach that offered corrections to enhance topographic

accuracy in complex terrains. Field measurements validate the rectified stereo-DEM's effectiveness against high-resolution LiDAR DEMs.

All these DEMs were used to model the Pettimudi debris flow. Debris flow modeling has evolved significantly since the 1960s, with numerical simulations and physical models used to predict critical parameters, including runout distances, sediment depth, and impact pressures (Fan et al., 2017; Zhang, 2019). Early studies focused on statistical or empirical relationships between landslide features and runout distances (Corominas, 1996; Rickenmann et al., 2006). Empirical models, such as the one developed by Chang et al. (2011) using multiple linear regression, provide quick estimates of debris flow volume using watershed area, landslide extent, geological conditions, and rainfall factors, aiding hazard assessment and model calibration. Numerical models, such as Rapid Mass Movement Simulation (RAMMS) (Christen et al., 2010), offer the advantage of estimating flow parameters, including height, velocity, and pressure, across irregular terrains from initiation to deposition, linking debris flow hazards to vulnerability and risk (Abraham et al., 2021; Frey et al., 2016; Hussin et al., 2012). Hence, in this study, we preferred RAMMS over other methods. Although we have used all the DEMs (stereo, rectified stereo, and LiDAR), the improved accuracy of the rectified stereo-DEM in runout simulations with RAMMS highlights its practical applicability for hazard assessment and mitigation. This replicable, cost-effective approach bridges the gap between traditional field surveys and advanced remote sensing technologies, providing a valuable solution for terrain modeling in resource-constrained settings and complex terrain.

2 | STUDY AREA

The Western Ghats, which run almost parallel to the western coast of India (Figure 1a), is one of the most prominent physiographic features of the Indian Peninsula, where rainfall-induced debris flows are typical during the monsoon months (Hao et al., 2020, 2022; Kuriakose et al., 2009). The region's prevailing tropical climate creates conditions conducive to debris flow (Kuriakose et al., 2009; Thampi, 1997). Historically, debris flows in the Western Ghats have been known for their devastation, with more extensive occurrences in recent years owing to extreme events (Ajin et al., 2022; Naidu et al., 2018; Vishnu et al., 2022). In 2018, Kerala (a southwestern state in India) faced severe consequences due to the aggravated monsoon rainfall, resulting in widespread landslides and floods (Agarwal, 2018; Martha et al., 2019; Megha et al., 2019; Parsa & Zehra, 2023; Sajinkumar et al., 2022; Sankar, 2018; Vishnu et al., 2019, 2020). According to Hao et al. (2020), the state witnessed approximately 4,728 landslides during a single storm event in August 2018, of which around 2,800 were debris flows initiated by shallow landslide failures. Out of the 4,728 landslides in the entire state of Kerala, 2,223 were confined to the hilly district of Idukki (Figure 1b).

This pattern continued in the monsoon seasons of 2019, 2020, and 2021, resulting in the unfortunate deaths of more than 160 people (Ajin et al., 2022), whereas the 2024 Wayanad landslide was the worst (~266 deaths) (Krishnapriya et al., 2024, 2025,b). On 6 August 2020, the torrential rainfall of 61.6 cm/day (Achu et al., 2021), the highest recorded in the area, triggered a debris flow in the Pettimudi village in Idukki district, Kerala (Sajinkumar & Oommen, 2020). The soil thickness in the region varies significantly, reaching a maximum of 16 m, and rests above the Precambrian basement, composed of high-grade metamorphic rock, including hornblende gneiss and pink granite gneiss (GSI, 2005).

This debris flow originated in a forested area and flowed across a tea plantation before debouching into the valley bottom, where the hutments of migrant tea plantation workers are situated (Sajinkumar & Oommen, 2021). The debris flow initiation is very near to the drainage divide, and the long run-out path of 1,200 m joins a second-order stream (Figure 1c). The area of the debris flow source, which was densely forested prior to the event, falls within the boundaries of the Eravikulam National Park; however, the debris-flow event largely removed the vegetation cover within the source zone. This Park comprises a significant portion of shola forests, including various species such as *Actinodaphne bourdilloni* (reaching heights of up to 10 m), *Microtropis ramiflora* (with heights ranging from 5 to 8 m), *Pittosporum tetraspermium* (reaching heights of up to 8 m), and *Sysygium aronottianum* (with heights ranging from 15 to 35 m) (Source: https://forest.kerala.gov.in/index.php/about-us/wildlife/2015-03-16-09-50-24/national-parks/eravikulam-national-park). The presence of large boulders of basement rocks above finer colluvial deposits, colluvial mantles along steep scarps (~2080 m amsl), and structurally controlled, vegetation-filled gullies observed in high-resolution imagery collectively indicate a history of slope instability and tectonic activity, highlighting the landslide-prone nature of the area.

3 | DATA AND METHODOLOGY

3.1 | Digital elevation models (DEM)

The pre-event DEM data were acquired on 5th December 2019, and the post-event DEM data were acquired on 22nd February 2023, encompassing the time of the debris flow at Pettimudi. The DEMs were derived from high-resolution WorldView imagery at 0.46 m resolution, operated by Maxar Technologies, using photogrammetric methods. The resultant DEM of 1 m spatial resolution provides detailed topographic conditions and eventually generates more derivatives such as slope, aspect, curvature, and drainage networks that help with the analyses of terrain, topography, and landscape characteristics (cf. Saleem et al., 2019), apart from volume estimation using the DEM of Difference (DoD) methods (cf. Atefi & Miura, 2021).

While analyzing the stereo-DEMs, errors were identified over the densely vegetated area. These errors were likely caused by interpolation across thick vegetation cover and limitations in vertical accuracy (approximately 0.5 m), particularly in forested areas and on steep slopes exceeding 20°, where the ground was obscured by forest. Such errors are common in stereo-DEMs because it is challenging to construct accurate terrain models using SfM techniques. This is more evident when such dense forest canopy is observed from spaceborne imagery and conventional camera angles, as it does not show adequate ground surface (Tuominen et al., 2015). An example of these errors is shown in Supporting Information S2, which highlights high negative DoD values indicating a depth of depletion up to 31.48 m, which is unacceptable compared to field observations. Thus, using on-site and LiDAR measurements of tree height and elevation differences from the field, we can effortlessly correct both pre- and post-event DEMs.

3.2 | Field data

Field study in Pettimudi was conducted from November 22nd to 25th, 2022. One traverse from the toe to the crown and several traverses across the debris flow were done during this fieldwork. The elevation differences throughout the debris flow run-out path were measured using a standard measuring tape wherever possible, and in inaccessible places (within 200 m) using a Hawke Optics LRF Pro 400 range meter. This range meter was validated at 25 locations using physically measured values, and both sets of values were found to agree. The location details (latitude and longitude), obtained using a Garmin eTrex 10 GPS (with a horizontal accuracy of 3.65 m), were verified with high-resolution Google Earth images and DGPS-GEOEXPLORER 6000 series.

3.3 | LiDAR digital elevation model

LiDAR data for the study region were collected in two stages using a DJI M300 UAV equipped with a Zenmuse L1 sensor. The Zenmuse L1 integrates a Livox AVIA solid-state LiDAR module, a high-accuracy Inertial Measurement Unit (IMU), and an RGB camera with a 1-inch Complementary Metal Oxide Semiconductor (CMOS) sensor, all mounted on a 3-axis stabilized gimbal. Flights were conducted at an altitude of 100 m above ground level (AGL), using terrain-following functionality to collect LiDAR point clouds. The initial flight focused on the debris flow source area, while the subsequent phase mapped the debris flow runout zones. An autonomous flight path was programmed using the DJI Pilot 2, leveraging Real-Time Kinematic (RTK) technology for precise positioning and navigation. The resulting LiDAR point cloud has a spacing of 244 points per square meter, while the RGB imagery achieves an effective Ground Sample Distance (GSD) of 3.27 cm per pixel. Subsequently, DJI Terra software was used to process the point clouds and generate an initial. las file, which was then imported into a Geographic Information System (GIS) environment to produce a 10 cm resolution DEM. This DEM was later resampled to 1 m for DoD.

3.4 | DEM correction

We have carefully combined LiDAR measurements and field-collected elevation values from multiple locations along the debris flow run-out path to ensure the highest level of accuracy in the pre- and post-event stereo-DEMs. This integration could effortlessly correct elevation variations in the specified locations. Thus, the pixel values in the DEM were improved by incorporating the field-collected elevation difference values, and a rectified stereo-DEM was generated for both the pre- and post-event from the field data points in a GIS environment.

Considering the diverse range of tree heights observed in the study area and LiDAR measurements, an elevation increase of around 15 m was observed in the vegetated areas. In the tropical evergreen forests of the Western Ghats, vegetation is highly heterogeneous and densely packed, making it impractical to identify and apply spatially varying canopy-height corrections at the required scale, unlike in plantation-type forests with more uniform structure; therefore, using an average height represents a practical and representative choice despite the diverse tree heights. Using a mean tree height for canopy correction in DEM rectification is a common practice in forested or inaccessible areas when high-resolution, continuous canopy data is unavailable (Kellndorfer et al., 2004). An average value of 15 m was thus used while correcting the pre-event DEM. The corrections were applied to the vegetation-covered area over the debris flow source using observed tree heights from the field and the UAV LiDAR dataset (Supporting Information S3) for both the pre- and post-event DEMs.

3.5 | Debris flow volume computation

The DoD is a pixel-by-pixel volume map with a horizontal resolution of 1 × 1 m, with each pixel value denoting the elevation difference between the pre- and post-event DEMs. Calculation of the depleted volume relies on identifying negative elevation differences from the DoD, indicating a reduction in height due to debris flow. These negative values are then multiplied by the pixel area (1 m^2) to determine the volume of eroded material. In contrast, the accumulated volume represents the quantity of material deposited along the flow path and within the accumulation zone, having been transported by debris flow. The disparity between the depleted and accumulated volumes is therefore interpreted as the net volume loss, representing material that was transported into the stream during the debris flow event and not retained within the deposition zone. Volume computation has been done using three different datasets: (i) pre- and post-event stereo-DEMs, (ii) rectified pre- and post-event stereo-DEMs, and (iii) rectified pre-event stereo-DEM and post-event LiDAR DEM.

3.6 | Debris flow simulation using RAMMS

The RAMMS::DEBRIS FLOW utilizes the Voellmy friction model (Salm, 1993; Voellmy, 1955), originally developed for snow avalanches and commonly used for debris flow back-analysis, to accurately simulate debris flow velocity and deposition thickness, accounting for high-speed, long-distance run-out (Hungr, 1995). Specifically, RAMMS::DEBRIS FLOW simulates debris flow in complex terrains (Mikoš & Bezak, 2021). Modelers can easily view and analyze simulation results with user-friendly visualization tools. These tools are great for understanding how the movement progresses from initiation to run-out within 3D landscapes. To run a simulation, users can choose between two options: one based on the release area and the other on the input hydrograph, depending on the type of flow. In cases involving channelized debris flows like Pettimudi, an input hydrograph may be more appropriate than specifying a block release, owing to the difficulty in identifying the initial source volume and the assumption of instantaneous material fluidization (Mitchell et al., 2021). RAMMS uses a friction model called Voellmy-fluid, which helps to understand how these flows behave. It divides frictional resistance into two components: dry-Coulomb friction (μ coefficient) scaled with normal stress and a velocity-squared drag or viscous-turbulent friction (ξ coefficient). These factors determine how fast the flow is moving: whether it is slowing down or speeding up. The two parameters μ and ξ of the Voellmy friction model govern the flow behavior, with μ dominating at low flow rates and ξ at high flow rates. Throughout the simulation, these factors stay constant within the calculation domain as RAMMS, operating

under a single-phase model, treats the material as a bulk flow without distinguishing between fluid and solid phases (WSL, 2022).

The RAMMS simulation of the Pettimudi debris flow uses the pre-event DEM to assess the impact of debris flow run-out across different zones, based on the depleted volume. The post-event DEM is used to assess the match with the RAMMS simulation. Accordingly, two simulations were done using the following datasets: (i) pre-event raw stereo-DEM and (ii) rectified stereo-DEM. A thorough assessment is then carried out by simulating the run-out path, before and after the rectification. The volume obtained from the DoD was used to derive the input hydrograph peak volume (cf. Rickenmann, 1999). Due to the complex composition of the actual debris flow, selecting appropriate friction parameters for an accurate RAMMS simulation was challenging. These parameters are critical for effective numerical simulation (Koçyiğit & Gürer, 2007), as they significantly affect the results (Bezak et al., 2019; Mikoš & Bezak, 2021; Zhang, 2019). The friction coefficients μ and ξ are calibrated in each case using raw and rectified stereo-DEMs until the simulation matches the actual flow path derived from post-event high-resolution Google Earth imagery. In the simulations, μ is defined as tan(α), where α is the slope angle in the deposition zone, where debris materials are carried from the event initiation to the deposition phase (WSL, 2022). The values 0.05, 0.1, and 0.2 were tested for μ based on field observations. ξ, which characterizes the turbulent behavior of the flow (WSL, 2022), is fine-tuned by testing values of 50, 100, 150, and 200 m/s^2. Generally, granular flows exhibit small ξ values, whereas muddy flows are often associated with larger ξ values (> 200 m/s^2). To further investigate the effect of DEM rectification, both DEMs were later simulated using the same friction coefficients ($\mu = 0.1$, $\xi = 100$ m/s^2) to isolate the influence of topographic correction on flow behavior. Comparing these simulations enabled a direct assessment of how DEM rectification improves run-out predictions and reduces uncertainty in debris flow modeling. Calibration was conducted using a trial-and-error approach (Hussin et al., 2012), systematically exploring a range of input parameters (see Supporting Information S4 for details). Based on preliminary simulations, a narrower parameter range was identified that reproduced the most realistic flow behavior, ensuring that the final calibrated parameters yielded model outputs consistent with the observed site conditions.

3.7 | Accuracy assessment

The measurements and quantifications of debris flow in each simulation are compared with the actual debris flow footprint to quantify True Positives (TP), False Positives (FP), True Negatives (TN), and False Negatives (FN). In the simulated outcome, the area corresponding to the real shape is identified as TP, while a simulation that wrongly predicts the flow that remains unaffected in reality is labeled FP. Conversely, if the flow occurs through an area but the model fails to predict it, it will be FN; and if the flow is absent in both the real and simulated cases, it will be TN. Using these values, sensitivity, specificity, and likelihood ratio were calculated. Sensitivity (Equation 1) measures the proportion of the actual area of the debris flow that is correctly identified as positive by the model.

$$Sensitivity = \frac{TP}{TP + FN} \quad (1)$$

Whereas specificity (Equation 2) measures the proportion of actual negative cases (areas without debris flow run-out) that are correctly identified as negative by the model.

$$Specificity = \frac{TN}{TN + FP} \quad (2)$$

The simulation is considered perfect if the sensitivity and specificity are 1 (Abraham et al., 2021; Kern et al., 2017). Also, the likelihood ratio (LR) (Equation 3) is a measure that assesses the diagnostic accuracy of a model.

$$Likelihood\ Ratio\ (LR) = \frac{Sensitivity}{1 - Specificity} \quad (3)$$

The higher the value of the likelihood ratio (LR), the better the model's ability to identify TP, indicating improved simulation performance. This comparison of run-out simulations using the DEMs before and after rectification validates the rectification process and ensures the accuracy of the simulation outcomes. The flowchart of the entire methodology for this study is shown in Figure 2.

4 | RESULTS

4.1 | DEM correction using field data and LiDAR measurements

Analysis of the DoD of pre- and post-event stereo-DEMs shows a higher elevation difference (~25 m) in areas adjacent to the source (near the scarp zone). These values are much higher than the field-verified values reported for the region (Figure 3a), where only a few meters of soil are reported (0.25–5 m; Abraham et al., 2019). This significant elevation difference could be due to dense vegetation cover in the area, suggesting the need for corrections before proceeding with any further debris flow analysis.

The DEM was rectified and enhanced using field-collected elevation data and LiDAR measurements. About 150 hand-measured and 35 range-meter-measured locations were incorporated into the raw stereo-DEM (Figure 3c–f). In addition to data collection, we captured high-resolution photographs. Soil thickness on inaccessible slopes and tree heights were measured at long range using a laser rangefinder (Figure 3e,f). Following rectification of the pre- and post-event stereo-DEMs, the DoD exhibited a more satisfactory depth of depletion of 7.08 m at the debris flow scarp, rectifying the initial value (Figure 3b). And, the rectified post-event stereo-DEM reduced elevation residuals by up to 0.45 m root mean square error (RMSE) compared to the pre-rectified post-event stereo-DEM.

4.2 | Debris flow volume computation

Debris flow volume computation was done (i) using DoD of pre- and post-event stereo-DEMs, and (ii) using DoD of rectified stereo-DEMs (Table 1). The volume calculated from the DoD using the initial stereo-DEMs yielded a volume depletion of 199,000 ± 20,000 m^3, while the DoD of the rectified stereo-DEMs showed a depletion volume of

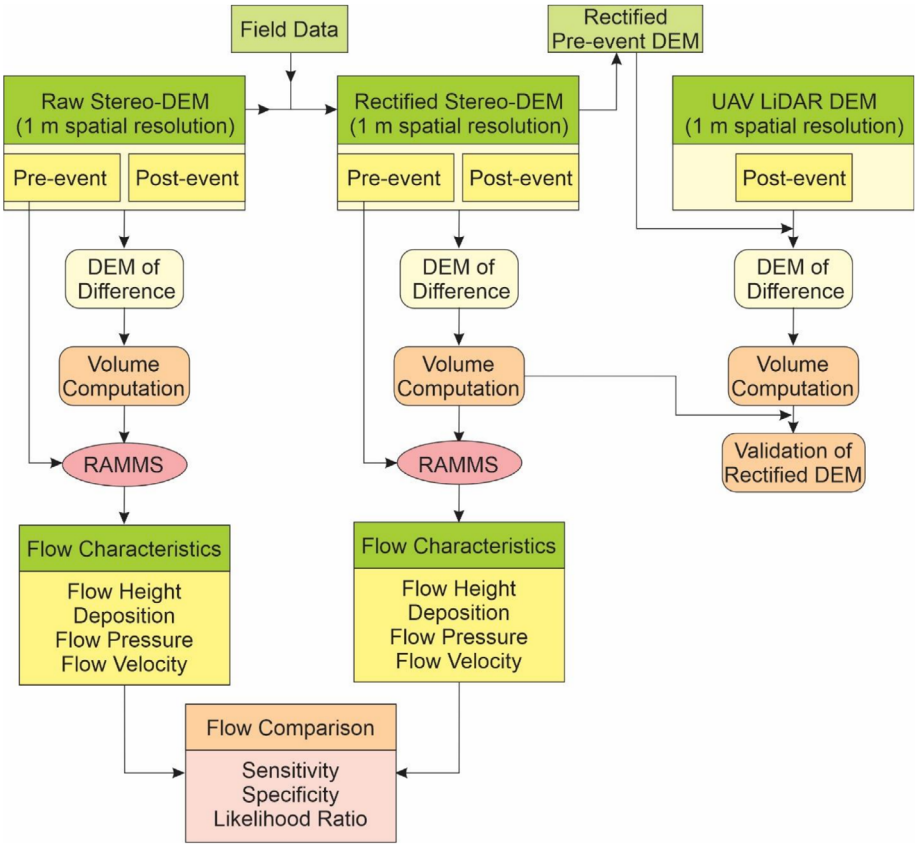

FIGURE 2 Flow chart showing the methodology adopted in the study.

170,000 ± 20,000 m^3. Additionally, the volumes of accumulation obtained from the DoD before and after rectification are 9,700 ± 1,400 m^3 and 24,600 ± 4,100 m^3, respectively. In both cases, the volume of debris depleted is significantly greater than the volume of accumulation because most landslide-derived material was not retained at the deposition site but was rapidly evacuated by the fluvial system. In steep, monsoon-fed catchments, landslides generate short-lived yet extreme sediment fluxes, leading to efficient downstream transport of debris during and immediately after the event (Yunus, Ishan, et al., 2025). In this case, the debris entered a first-order stream and was temporarily deposited on a locally widened valley floor at the base of the slope, rather than forming a classical alluvial fan by an abrupt reduction in gradient. The direct connectivity to the tributary of the Periyar River limited long-term sediment storage despite the wider deposition zone, and a minor fraction of the temporarily deposited material may have been reworked during subsequent rainfall events. The results also reveal that while the volume of depletion decreased by 14.42% from raw stereo-DEMs to rectified stereo-DEMs, the volume of accumulation increased by 54.16% (Figure 4). When comparing the volume of accumulation before and after rectification, the initial stereo-DEM missed some areas of accumulation along the flow path, which were incorporated in the rectified stereo-DEM using field measurements, leading to an increase in the volume of accumulation.

4.3 | Debris flow simulation

Simulation of debris flow using RAMMS was done for two conditions: before and after rectification, i.e., (i) using the initial raw pre-event stereo-DEM, and (ii) using the rectified pre-event stereo-DEM. Initially, the 1 m resolution pre-event stereo-DEM was used to simulate the run-out path of this debris flow using the calculated volume of depletion (from the DoD before rectification), i.e., 198726.59 m^3 for an initial peak hydrograph volume (cf. Rickenmann, 1999), with the dry coulomb type (μ) and viscous turbulent (ξ) friction values (0.1 and 50 m/s^2, respectively) calibrated until the flow path coincides with the original flow path. The results of the run-out modeling showed a maximum flow height of 12.29 m along the flow path and a maximum deposition of 8.20 m in the accumulation zone. Based on this modeling, the debris flow reached a maximum velocity of 12.37 m/s along its thalweg, with a simulated maximum flow pressure of 305.93 kPa (Figure 5a-d).

Subsequently, the 1 m resolution rectified pre-event stereo-DEM was modeled with an initial peak hydrograph volume of 170061.33 m^3 for debris flow using friction coefficients $\mu = 0.1$ and $\xi = 100$ m/s^2, calibrated until the run-out matched the actual flow path. The results of run-out modeling using the DoD volume from rectified stereo-DEMs showed a maximum flow height of 14.04 m and a maximum deposition of 7.53 m, both at the zone of accumulation. The debris flow reached a maximum velocity of 12.94 m/s along its thalweg, with a simulated maximum flow pressure of 334.81 kPa (Figure 5e-h). High flow velocity and pressure were observed in the depletion zone, where the slope angle is steep enough for depletion. As the debris flow simulation reached the flat surfaces, the slope angle decreased, causing a simultaneous drop in flow pressure and velocity, leading to debris deposition and formation of a deposition zone.

4.3.1 | Assigning values for friction parameters μ and ξ

After calibration of μ with values as 0.05, 0.1, and 0.2 through comparison of the simulated flow path and flow height with actual field

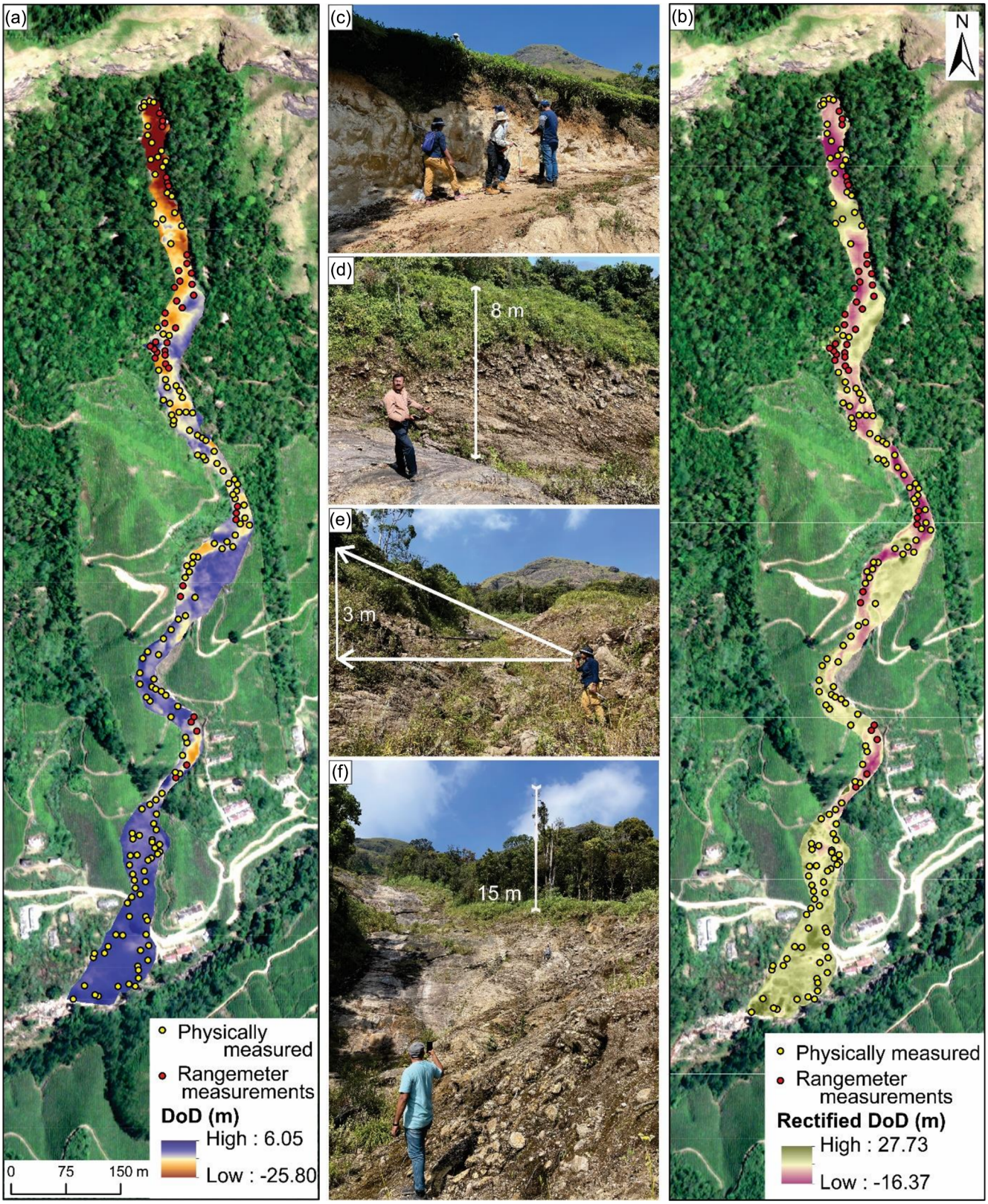

FIGURE 3 **(a)** DEM of difference (DoD) of raw pre-event stereo-DEM **(b)** DoD of rectified pre- and post-event stereo-DEM (Source of 3a-b: WorldView-2 Imagery © 2023 DigitalGlobe, Inc., a Maxar company) **(c)** analysing the weathered column on the flanks of the debris flow **(d)** physically measuring the depth of depletion at a location in the debris flow **(e)** measuring the depth of depletion using a range meter **(f)** analysing the soil thickness and tree heights in the scarp region of the debris flow.

observations, we set μ to 0.1 ($\alpha \approx 5.7°$) (Figure 6). We fine-tuned ξ by adjusting it to 50, 100, 150, and 200 m/s^2. For each release volume before and after DEM rectification, two ξ values were calibrated as 50 m/s^2 (for the release volume of 198726.59 m^3, before rectification) and 100 m/s^2 (for the release volume of 170061.33 m^3, after rectification).

Furthermore, to assess the influence of ξ, we examined its sensitivity to output flow characteristics (Figure 7), particularly the

TABLE 1 Table showing the volume computation of landslide using different DEM combinations: pre- and post-event stereo-DEMs, rectified pre- and post-event stereo-DEMs, and rectified pre-event stereo-DEM and post-event LiDAR DEM.

Before rectification		After rectification		For validation of DEM rectification	
Volume calculated using the DoD of pre- and post-event stereo-DEMs (m^3)		Volume calculated using the DoD of rectified pre- and post-event stereo-DEMs (m^3)		Volume calculated using the DoD of rectified pre-event stereo-DEM and post-event LiDAR DEM (m^3)	
Depletion	1,98,726.59	Depletion	1,70,061.33	Depletion	1,69,856.33
Accumulation	9,663.78	Accumulation	24,561.10	Accumulation	24,561.10
Loss	1,89,062.81	Loss	1,45,500.23	Loss	1,45,295.23

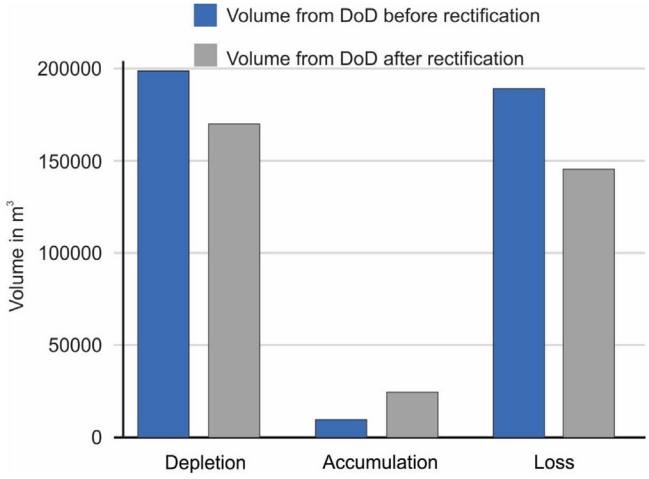

FIGURE 4 Figure showing the histogram of volume of depletion, accumulation, and loss computed from the DoD before and after rectification.

maximum velocity at three points along the flow path: the scarp, the middle of the flow path, and the deposition zone where the hutments were destroyed. By analyzing the maximum velocity at these points for varying ξ values via simulation, we aimed to determine the uncertainty in velocity due to small changes in ξ. So, we used the rectified pre-event stereo-DEM to simulate the debris flow with $\mu = 0.1$ and ξ values of 50, 100, and 150. The value of ξ determines the rate of flow; as we increase its value, the flow accelerates due to reduced friction (cf. Abraham et al., 2021). However, changes in ξ do not uniformly correlate with changes in velocity throughout the flow path, as the velocity variations are not consistent (Figure 7). A 50% decrease or increase in ξ value (i.e., 50 or 150 m/s^2) from the one ($\xi = 100$ m/s^2) that matches the actual debris flow path does not reciprocate the same decrease or increase in velocity values in every observed point. The ξ value shows varying sensitivity in different locations (scarp with +8% and −12%, middle of the flow path with +40% and −35%, deposition zone with +22% and −32%). This variability reflects the underlying model behavior, in which ξ governs the velocity-dependent viscous-turbulent resistance, which scales with the square of the flow velocity (Zhang, 2019). Even modest changes in ξ can cause disproportionately large or small effects on flow dynamics, depending on local slope, confinement, and flow depth (Salm, 1993). As a result, small changes in ξ can lead to non-linear and location-specific variations in velocity (Salm, 1993; Voellmy, 1955; Zhang, 2019). The asymmetric responses observed across the scarp, channel, and deposition zones highlight the system's sensitivity to local slope, flow depth, and channel geometry. Unlike the dry Coulomb friction coefficient (μ), ξ plays a more dominant role in steep or confined sections with higher flow energy (Kumar et al., 2024). These inconsistencies highlight the need for ξ calibration for each DEM and debris volume, reinforcing that accurate simulation outcomes require case-specific parameter tuning, particularly in complex terrains. Fine-tuning the value of ξ is therefore important for precise flow simulations and for understanding its sensitivity and influence on the accurate prediction of debris flow behavior.

4.4 | Accuracy assessment

Run-out simulations with both DEMs, using the same friction parameters ($\mu = 0.1$, $\xi = 100$ m/s^2), assess the effectiveness of the rectification process by comparing simulated outcomes with real-world debris flow scenarios. The simulations' sensitivity and specificity relative to the actual flow path are similar for both the rectified and raw stereo-DEMs. However, LR is higher for the simulated outcome with rectified stereo-DEM than for raw stereo-DEM (Table 2). Sensitivity, which measures the simulation's ability to correctly identify debris flow paths (positives), is 0.97 for both simulated outcomes. FN, which controls sensitivity, is very low in both simulations, yielding better sensitivity values. Similarly, specificity, indicating the model's ability to correctly identify non-debris flow areas (negatives), improved slightly from 0.90 to 0.91 after rectification. With an increase in LR from 9.99 to 11.36, the rectified stereo-DEM simulation demonstrates a higher ability to discriminate between debris flow and non-debris flow areas compared to the raw stereo-DEM simulation. This enhancement suggests that the rectified stereo-DEM captures subtle variations more effectively, leading to a more accurate depiction of actual debris flow paths. Also, the run-out modeled using rectified pre-event stereo-DEM demonstrated better spatial agreement with the observed debris flow path, improving the runout overlap accuracy from 91% to 92% relative to the raw pre-event stereo-DEM. Thus, the confusion matrix indicates that the simulation with the rectified stereo-DEM is better than that with the raw stereo-DEM, which is affected by inaccuracies.

5 | DISCUSSION

5.1 | Pettimudi: one of the biggest debris flows in the Western Ghats

Debris flows in complex mountainous terrains such as the Western Ghats are influenced by a combination of geological, geomorphological, and climatic factors (cf. Krishnapriya, Rajaneesh, et al., 2025). Given the increasing frequency and intensity of debris flows in recent years (Ajin et al., 2022), it is essential to systematically investigate and

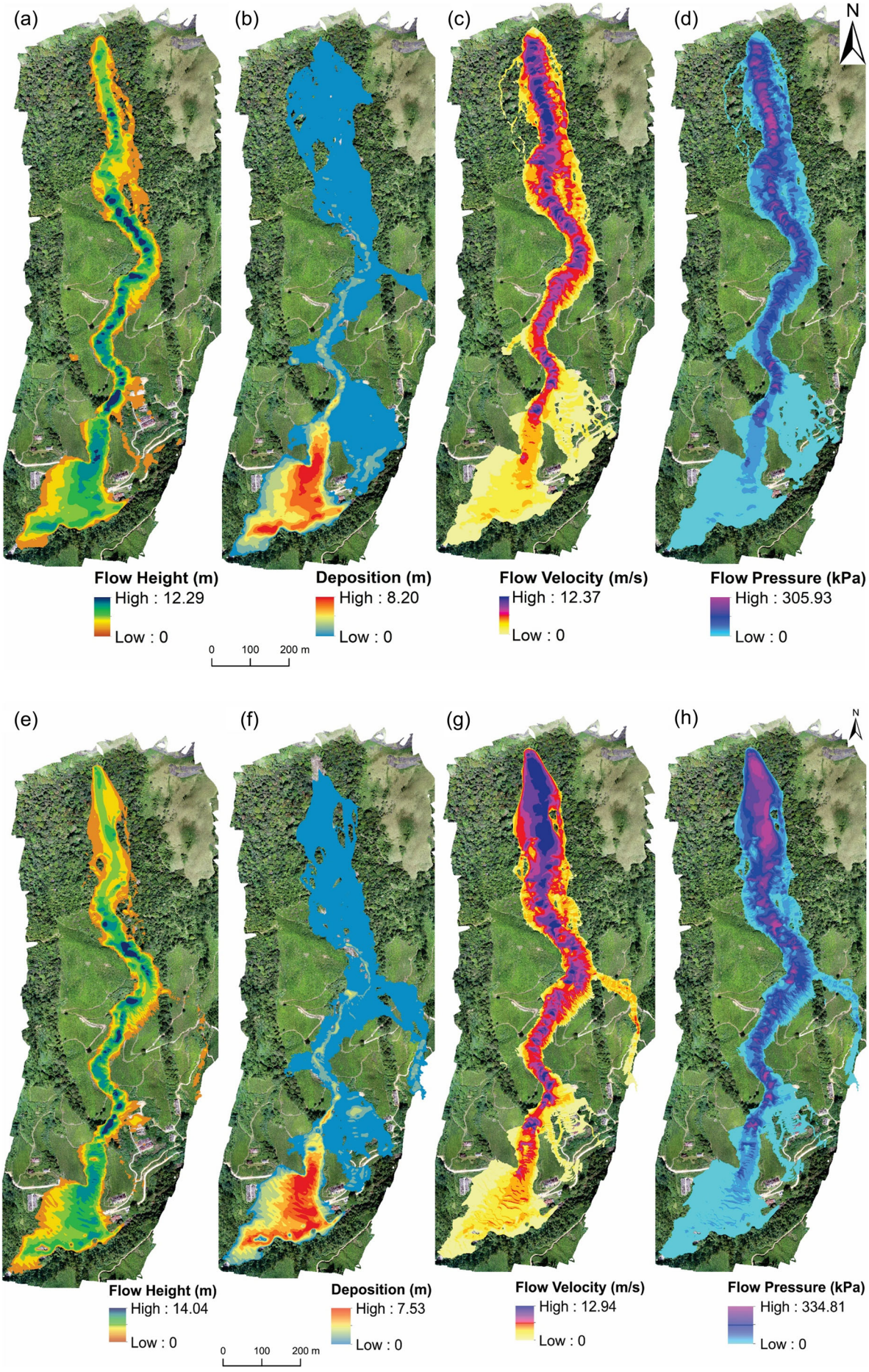

FIGURE 5 Legend on next page.

FIGURE 5 Flow characteristics of the Pettimudi landslide simulated from the raw pre-event stereo-DEM before rectification **(a)** flow height (m) **(b)** deposition (m) **(c)** flow velocity (m/s) **(d)** flow pressure (kPa); flow characteristics of the Pettimudi landslide simulated from the rectified pre-event stereo-DEM after rectification **(e)** flow height (m) **(f)** deposition (m) **(g)** flow velocity (m/s) **(h)** flow pressure (kPa) (Source: UAV RGB Image).

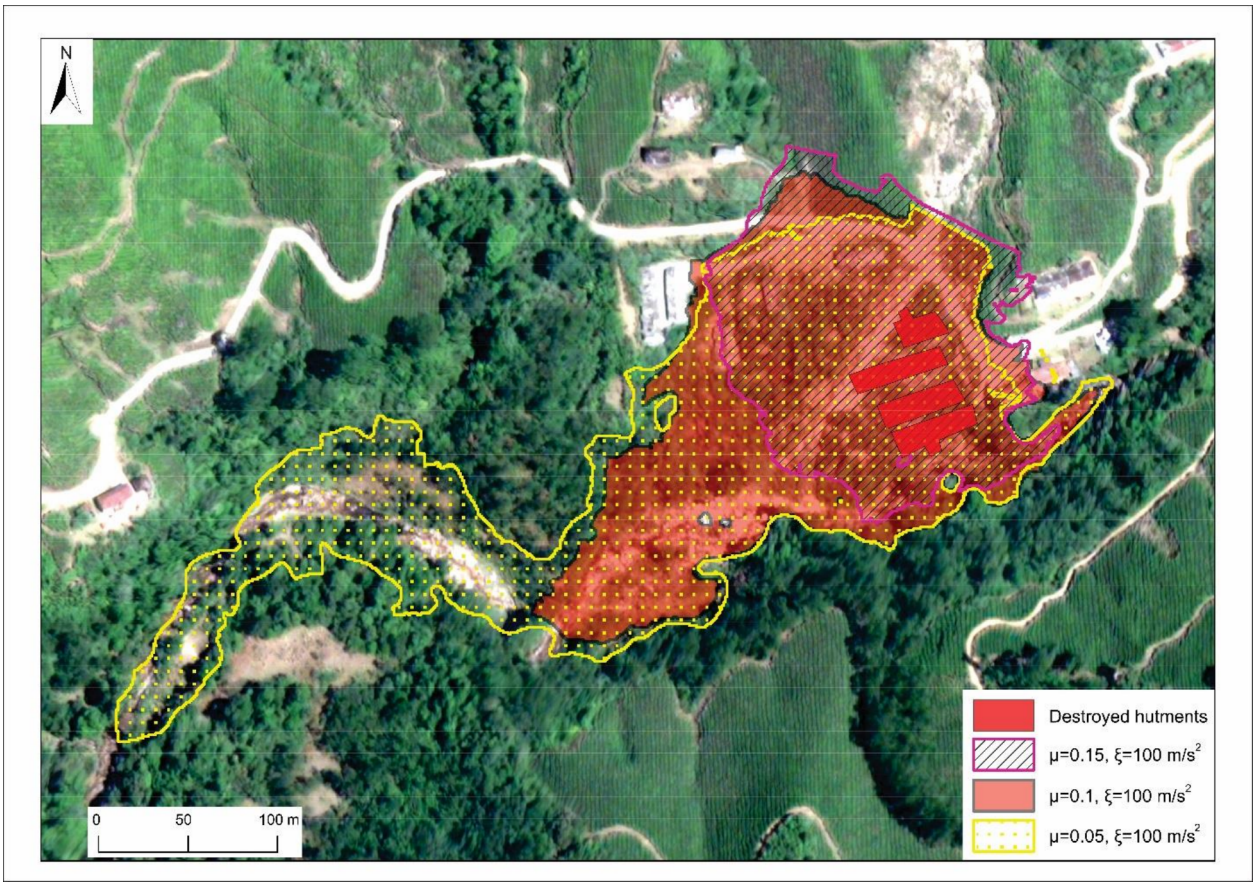

FIGURE 6 Figure showing three flow paths simulated with values of $\mu = 0.05, 0.1, 0.15$, and $\xi = 100$ m/s^2 at the zone of deposition, where $\mu = 0.1$ matching with the actual extent of the debris flow (Source: WorldView-2 imagery © 2023 DigitalGlobe, Inc., a Maxar company).

monitor these hazards. The Pettimudi debris flow of 2020 stands out as one of the deadliest and most destructive in the Western Ghats, particularly for its massive scale, high velocity, and devastating impact on human settlements. This event, like many debris flows in forested or uninhabited areas of the Western Ghats, swiftly debouched in a populated tea estate, claiming the lives of marginalized people. Its importance also lies in its classification as a typical debris flow, with a long run-out and significant volume, flowing rapidly along a structurally controlled first-order stream. While preliminary studies provided an initial estimate of the debris flow volume of 280,500 m^3 (Achu et al., 2021), the DoD method in this study offered a more refined, data-driven assessment (~170,061 m^3), highlighting the advantage of high-resolution topographic analysis in post-event volume estimation. Similar to Pettimudi, catastrophic debris flows within forested regions continued in 2024, where the Wayanad debris flow event (11°27′57.07″N, 76°8′9.91″E), which is the largest in recent history, resulted in an estimated sediment loss of 5.1–5.7 $\times 10^6$ m^3 (Krishnapriya et al., 2024; Krishnapriya, Amrutha, et al., 2025; Yunus, Sajinkumar, et al., 2025). Both debris flows initiated after intense, short-duration, high-intensity monsoon rainfall, during which weathered soil columns were saturated, leading to failure. Another debris flow at Irshalwadi (18°55′58.23″N, 73°14′4.17″E), with an estimated volume of 1.77 $\times 10^5$ m^3 (Baile et al., 2025), was triggered by over 500 mm of 3-day antecedent rainfall and involved precursory slope creep in porous basaltic terrain (Jain et al., 2024). These events underscore the challenges of studying debris flows on steep, forest-covered slopes of the Western Ghats and highlight the importance of integrating field-based investigations with remote sensing technologies for effective and reliable hazard assessment.

5.2 | Refining high-resolution DEMs in the Western Ghats: challenges and correction strategies

Utilizing remote sensing technology to extract information offers significant advantages (Xia et al., 2021), including the accurate extraction of information on debris flows, which is pivotal for early hazard prevention. High-resolution DEMs will be highly beneficial in such cases. In debris-flow-prone terrains like the Western Ghats, DEM rectification is essential, as several errors can creep in due to the thick canopy. Such interference impacts the accuracy of terrain representation. This goes unnoticed if unaware of field conditions. Thus, only the rectified

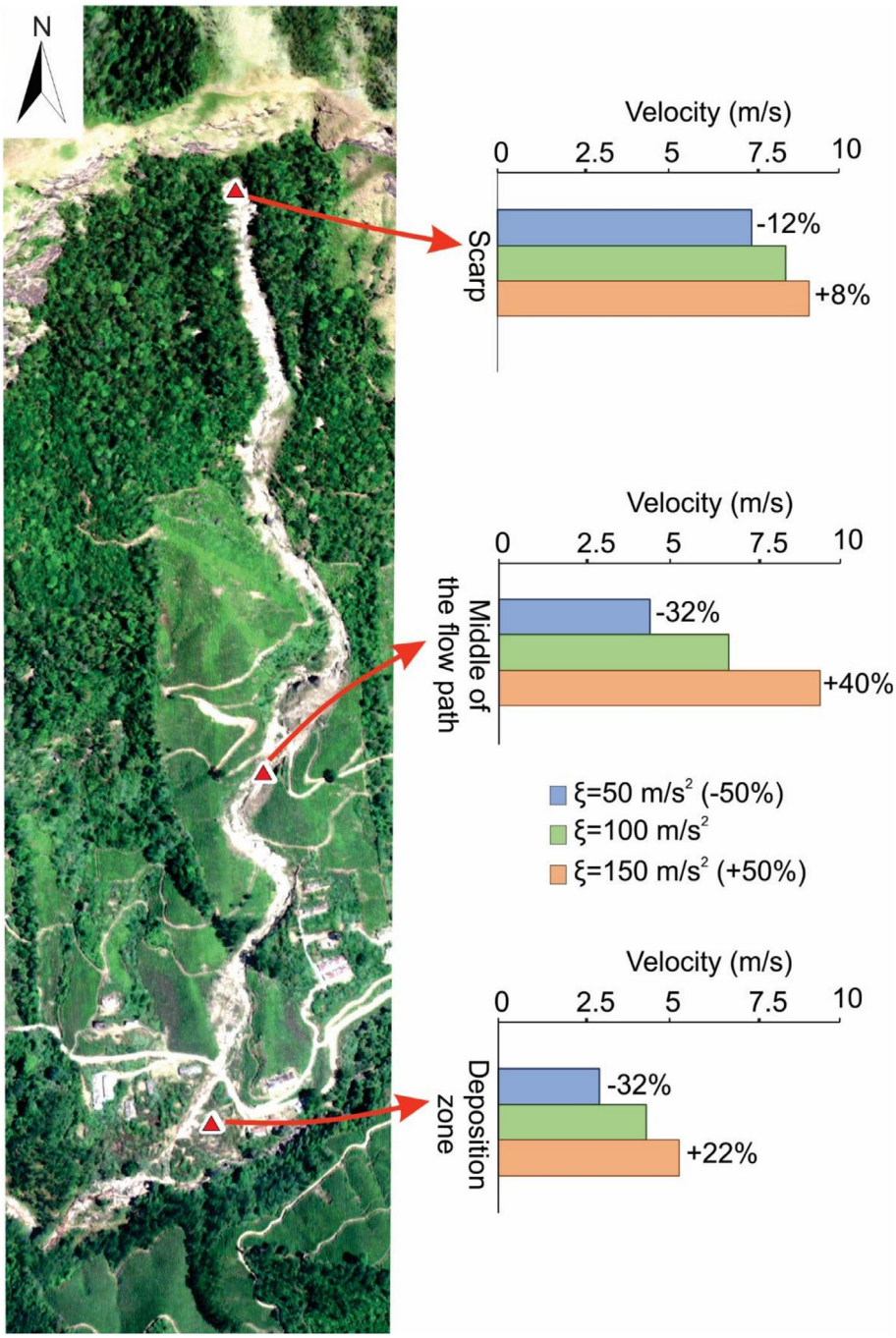

FIGURE 7 Sensitivity of velocity with values of $\xi = 50$, 100 and 150 m/s^2 and $\mu = 0.1$, at different points from the flow path: scarp, middle of the flow path, and deposition zone where the hutments were destroyed (Source: WorldView-2 Imagery © 2023 DigitalGlobe, Inc., a Maxar company).

TABLE 2 Confusion matrix of the area of simulated outcomes using the stereo-DEMs before and after rectification with the actual footprint of the debris flow.

		Statistical analysis of the simulation outcomes using	
		Raw stereo-DEM (m^2)	Rectified stereo-DEM (m^2)
	TP	**63618.1**	**63417.7**
	FN	**1668.7**	**1869.2**
	FP	**54268.9**	**47643.3**
	TN	**502,063**	**509,664**
Sensitivity	TP/(TP + FN)	0.97	0.97
Specificity	TN/(TN + FP)	0.90	0.91
Likelihood Ratio (LR)	Sensitivity/(1-Specificity)	9.99	11.36

DEMs can accurately capture the topographic features that influence debris flow occurrence in such tropical regions. Additionally, by incorporating rectified DEMs into run-out modeling, researchers can simulate and predict the extent and trajectory of debris flows. This is what was demonstrated in this study using Pettimudi debris flow as a case study.

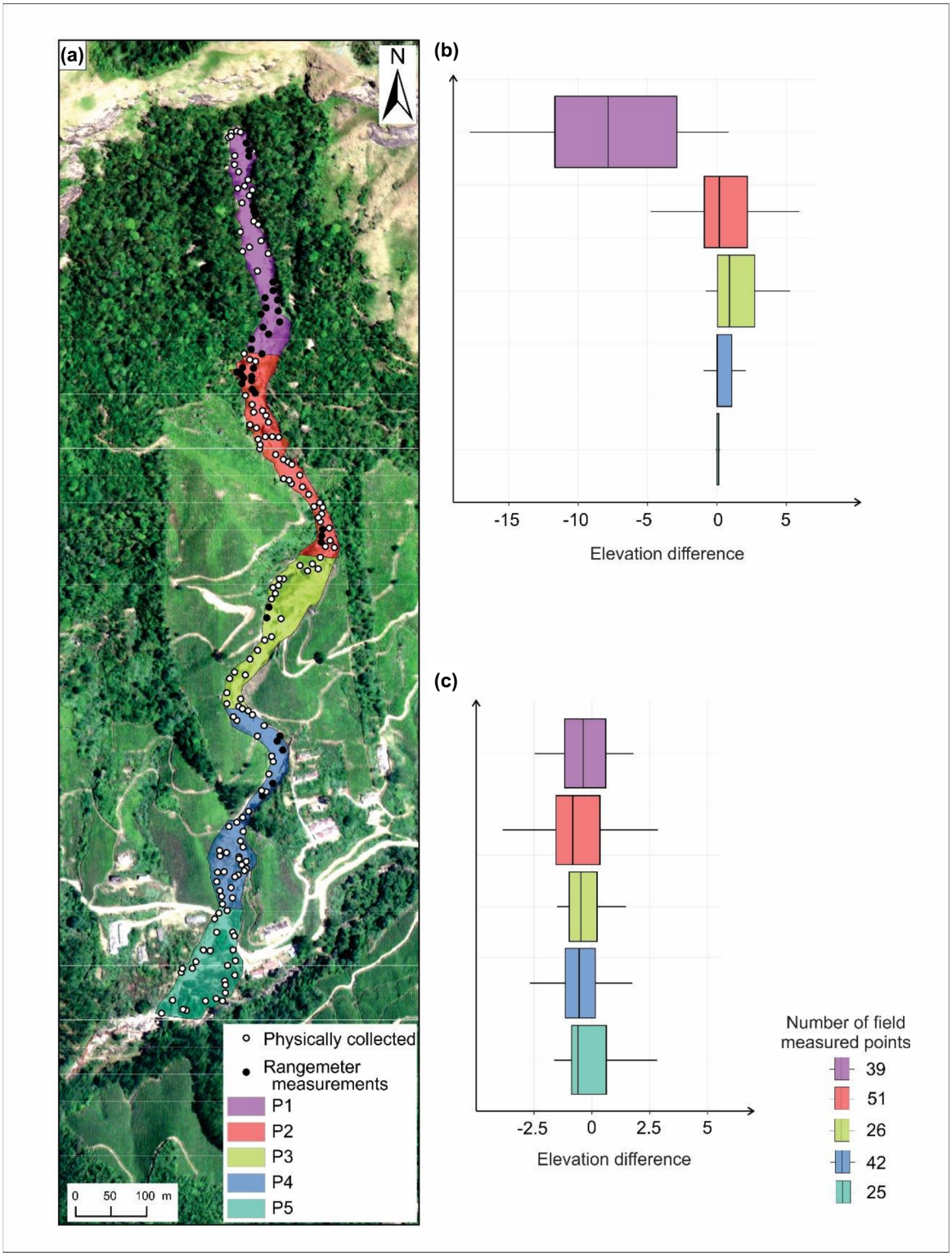

FIGURE 8 **(a)** Debris flow area with physically collected and range meter measured (field data) points (Source: WorldView-2 imagery © 2023 DigitalGlobe, Inc., a Maxar company) **(b)** box plots showing elevation differences between pre-event raw stereo and rectified stereo-DEMs **(c)** box plot showing elevation differences between raw stereo-DEM and rectified post-event stereo-DEMs, across different sections (P1 to P5) of the landslide.

The 1 m resolution pre- and post-event high-resolution stereo-DEM of the Pettimudi debris flow area was derived from the WorldView series. DoD of initial stereo-DEMs indicated a depth of depletion much greater than what was observed in the field, making it necessary to rectify the stereo-DEM to obtain accurate data. Many of the discrepancies were due to tree height. The high-volume quantification from the initial stereo-DEM is suspected to be due to considering canopy height as soil thickness, especially in the scarp area. The tree height in the area is ∼15 m (see section 3.4). This required local knowledge and field-based data collection, and thus, a field survey was conducted. The fieldwork was successful only in November 2022, with prior missions in November 2021 and January

2022 failing due to inaccessibility, as dumped materials in precarious conditions impeded access to several locations. The fieldwork enabled us to rectify the elevation difference through accurate on-site measurements using 150 physically measured points and 35 range-meter-validated points. To visualize the relation between the density of field data and the improvement in the pre-and post-event stereo-DEMs after rectification, we have divided the debris flow footprint into five equal parts, with the different numbers of the field measurement points in each of them (Figure 8a). Starting from the scarp to toe, the five parts are named P1, P2, P3, P4, and P5 with 39, 51, 26, 42, and 25 field measurements, respectively. Each box shows the distribution of elevation differences reduced from pre-rectified to rectified stereo-DEMs, which can be considered an improvement. Each part with a different number of field measurement points shows a different range of improvement after rectification.

Figure 8b shows the improvement in the pre-event stereo-DEM with the box plot of five parts with varying densities of field measurement points. Negative values of improvement indicate that the exaggeration of tree heights in the DEM has been removed, resulting in a decrease in elevation relative to the raw pre-event stereo-DEM. Since P1 comprises dense vegetation in the raw pre-event stereo-DEM, and the rectification process was substantially influenced in this area, its interquartile range is greater than that of the others and includes high negative values. For P3 and P4, most of the improvement is in positive values, indicating that the raw stereo-DEM has elevation values lower than the real-world condition, which may be due to a vegetative correction applied throughout the DEM during the company's photogrammetric correction. P5, the accumulation zone, showed the least improvement after rectification. Sections with more field measurements (P2, P4, P1, in decreasing order) exhibit more reliable improvements, confirming that a higher density of field data yields more accurate DEM corrections. A wide range of elevation differences between the pre-event raw stereo- and rectified stereo-DEMs suggests that significant adjustments were made to correct the pre-event stereo-DEM.

Figure 8c shows the box plot of the improvement in the rectified post-event stereo-DEM relative to the raw post-event stereo-DEM. All sections have nearly identical interquartile ranges, indicating consistent elevation correction. A narrower range of elevation differences between the post-event raw stereo- and rectified stereo-DEMs indicates that both these post-event stereo-DEMs closely match. It may be due to vegetation removal by the debris flow, and the error from the vegetation effect is minimal. Additionally, the time lag between pre- and post-event stereo-DEM data collection underestimated the eroded materials in subsequent erosion, highlighting the need for timely data acquisition in debris flow analysis.

5.3 | Calibration of friction parameters (μ and ξ values) in RAMMS and accuracy assessment

Calibration of friction parameters (μ and ξ) in RAMMS simulations, for both raw and rectified pre-event stereo-DEMs, underscores the critical role of parameter tuning for accurate debris flow modeling. The calibration process involved setting μ to 0.1, corresponding to the slope angle in the deposition zone, and adjusting ξ to account for the flow's turbulent behavior. Initial simulations with the raw stereo-DEM, using a release volume of 198726.59 m^3, required a ξ value of 50 m/s^2 to align the simulated flow path with the actual debris flow. In contrast, the rectified stereo-DEM, using a corrected volume of 170061.33 m^3, necessitated a higher ξ value of 100 m/s^2. A higher release volume generally results in a greater mass of material being mobilized, potentially leading to increased flow acceleration. As the flow becomes more massive and gains momentum, the frictional forces acting on it also increase. To accurately simulate this behavior, the ξ value must be adjusted accordingly. The lower ξ value for higher release volume effectively reduces the simulated flow acceleration, ensuring that the modeled behavior aligns with observed real-world dynamics. Conversely, for smaller release volumes, a higher ξ value is required to account for the lower frictional forces and less turbulent flow. This adjustment underscores the sensitivity of ξ to different release volumes and its impact on flow velocity.

Accuracy assessments comparing simulations with consistent friction parameters ($\mu = 0.1$, $\xi = 100\ m/s^2$) for both stereo-DEMs showed that the rectified stereo-DEM provided better discrimination between debris flow and non-debris-flow areas. The slight improvement in specificity and the higher likelihood ratio for the rectified stereo-DEM simulation indicated a more accurate representation of actual debris flow paths. The enhanced accuracy of rectified stereo-DEM in volume estimation and flow path prediction underscores the importance of thorough field verification and precise parameter tuning in debris flow modeling.

Calibration of the friction coefficients (μ and ξ) for debris flow modeling in our study aligns closely with the findings of Jain et al. (2021) and Abraham et al. (2021), demonstrating the reliability of these parameters in accurately modeling debris flow dynamics in the region. The friction coefficients calibrated for the Kurichermala debris flow by Abraham et al. (2021) were $\mu = 0.01$ and $\xi = 100\ m/s^2$, reflecting fluid-dominated flow behavior with minimal friction and highlighting the importance of fine particles and rapid flow dynamics. Similarly, the simulation of the Pettimudi debris flow by Jain et al. (2021) exhibited $\mu = 0.08$ and $\xi = 200\ m/s^2$, suggesting terrain-specific influences such as soil composition, slope, and flow dynamics. Compared to other studies in similar terrains, our calibrated values are consistent with friction parameters observed in fluid-dominated flows in Kerala's Western Ghats (Jain et al., 2021). These results further affirm the need for localized calibration to account for variations in geomorphology and rheological behavior.

5.4 | Validation of DEM rectification using UAV LiDAR survey

To showcase the efficiency of the methods, we conducted an additional field survey using the UAV LiDAR technique on 15–19 January 2024. The high-resolution post-event LiDAR DEM and the field-modified pre-event stereo-DEM were further processed to quantify the volume. This has given a value of 169856.33 m^3, close to the depletion volume derived from the DoD of the rectified stereo-DEMs, which is 170061.33 m^3. The rectified stereo-DEMs reduced the volume overestimation by approximately 99% compared to the pre-rectified stereo-DEMs. Comparison of DoD from the rectified pre-event stereo-DEM with both the rectified post-event stereo-DEM and the post-event UAV LiDAR DEM yielded nearly identical results,

validating the rectification process. This outlines the importance of calibrating the DEM using field data to accurately quantify volume and simulate the flow path, preventing potential misinterpretations of the catastrophe. Thus, the combination of field knowledge, on-site work, and advanced technology has enabled us to successfully quantify the volume of depleted material and model the debris flow.

6 | CONCLUSION

Using field data, we enhanced the accuracy of a high-resolution stereo-DEM, and used it to quantify volume and simulate the Pettimudi debris flow with the RAMMS model. This improvement involved incorporating field-collected elevation-difference data to correct errors in tree height. The rectified stereo-DEM, with friction parameters $\mu = 0.1$ and $\xi = 100$ m/s^2, demonstrated improved accuracy in capturing the actual debris flow footprint. This highlights the importance of thorough field verification and careful parameter tuning for reliable simulations for effective debris flow prediction. Furthermore, an independent UAV LiDAR mapping and its results also correlated with our results and showcased the advantage of our methodology. Thus, this method of rectifying DEM using field data could be ideal for studying debris flow in different regions. In conclusion, our novel field-based rectification methodology, validated against UAV LiDAR DEM data, provides a reliable approach to improve the accuracy of high-resolution DEMs, particularly in regions with variable tree heights such as tropical forests. Thus, this methodology offers a more reliable alternative to relying solely on default or hypothetical input parameters, thereby enhancing the credibility of debris flow hazard assessments in challenging terrain.

ACKNOWLEDGMENTS

The research was part of the BGS International NC programme 'Geoscience to tackle Global Environmental Challenges' (NERC reference NE/X006255/1). All authors acknowledge the Kerala State Disaster Management Authority (KSDMA) for granting permission to do fieldwork. The authors acknowledge the officials of Devikulam Taluk Office, SDMA (Idukki district), and Kannan Devan Hills Plantations Company (P) Limited for granting permission to fly UAV. Authors also thank the Editor-in-Chief, Prof. Stuart Lane, and two anonymous reviewers for constructive comments. KVK acknowledge the Department of Social Justice and Empowerment (NSFDC/E-81088), and SKS and YPA acknowledge the Indian Space Research Organization (ASCB/AS/2023/06) for funding.

CONFLICT OF INTEREST STATEMENT

The authors declare that they have no known competing financial interests or personal relationships that could have appeared to influence the work reported in this paper.

DATA AVAILABILITY STATEMENT

All the data are shared in Zenodo (10.5281/zenodo.14948464).

ORCID

Sajinkumar K. S. https://orcid.org/0000-0002-6461-8112
Yunus P. Ali https://orcid.org/0000-0001-9545-0714
Majdi Mansour https://orcid.org/0000-0003-3058-8864

REFERENCES

Abraham, M.T., Pothuraju, D. & Satyam, N. (2019) Rainfall thresholds for prediction of landslides in Idukki, India: an empirical approach. *Water*, 11(10), 2113. Available from: https://doi.org/10.3390/w11102113

Abraham, M.T., Satyam, N., Reddy, S.K.P. & Pradhan, B. (2021) Runout modeling and calibration of friction parameters of Kurichermala debris flow, India. *Landslides*, 18(2), 737–754. Available from: https://doi.org/10.1007/s10346-020-01540-1

Achu, A.L., Joseph, S., Aju, C.D. & Mathai, J. (2021) Preliminary analysis of a catastrophic landslide event on 6 august 2020 at Pettimudi, Kerala state, India. *Landslides*, 18(4), 1459–1463. Available from: https://doi.org/10.1007/s10346-020-01598-x

Agarwal, R. (2018) Lesson learned from killer floods in Kerala: time for retrospection. *Management and Economics Research Journal*, 4(2), 268–280. Available from: https://doi.org/10.18639/MERJ.2018.04.735013

Ait-Lamallam, S., Lamrani, R., Mastari, W. & Kechna, M. (2025) Effective strategies for mitigating the "bowl" effect and Optimising accuracy: a case study of UAV photogrammetry in corridor projects. *Drones*, 9(6), 387. Available from: https://doi.org/10.3390/drones9060387

Ajin, R.S., Nandakumar, D., Rajaneesh, A., Oommen, T., Ali, Y.P. & Sajinkumar, K.S. (2022) The tale of three landslides in the Western Ghats, India: lessons to be learnt. *Geoenvironmental Disasters*, 9(1), 16. Available from: https://doi.org/10.1186/s40677-022-00218-1

Allen, P.A. & Hovius, N. (1998) Sediment supply from landslide-dominated catchments: implications for basin-margin fans. *Basin Research*, 10(1), 19–35. Available from: https://doi.org/10.1046/j.1365-2117.1998.00060.x

Aristizábal, E., Martínez-Carvajal, H. & García-Aristizábal, E. (2017) Modelling shallow landslides triggered by rainfall in tropical and mountainous basins. In: Mikoš, M., Casagli, N., Yin, Y. & Sassa, K. (Eds.) *Advancing culture of living with landslides: Proceedings of the 4th World Landslide Forum (WLF)*, vol. 2. Cham, Switzerland: Springer International Publishing. Available from: https://doi.org/10.1007/978-3-319-53485-5_23

Atefi, M.R. & Miura, H. (2021) Volumetric analysis of the landslide in Abe Barek, Afghanistan based on nonlinear mapping of stereo satellite imagery-derived DEMs. *Remote Sensing*, 13(3), 446. Available from: https://doi.org/10.3390/rs13030446

Baile, A., Jha, M., Jain, N., Tignath, S. & Kinattinkara, R. (2025) Integrated landslide analysis using petrological investigation and drone based high resolution geospatial assessment: Irshalwadi landslide-a case study from Western Ghats of India. *Natural Hazards*, 121(1), 405–421. Available from: https://doi.org/10.1007/s11069-024-06826-4

Bezak, N., Sodnik, J. & Mikoš, M. (2019) Impact of a random sequence of debris flows on torrential fan formation. *Geosciences*, 9(2), 64. Available from: https://doi.org/10.3390/geosciences9020064

Boreggio, M., Bernard, M. & Gregoretti, C. (2022) Does the topographic data source truly influence the routing modelling of debris flows in a torrent catchment? *Earth Surface Processes and Landforms*, 47(8), 2107–2129. Available from: https://doi.org/10.1002/esp.5366

Chang, C.W., Lin, P.S. & Tsai, C.L. (2011) Estimation of sediment volume of debris flow caused by extreme rainfall in Taiwan. *Engineering Geology*, 123(1–2), 83–90. Available from: https://doi.org/10.1016/j.enggeo.2011.07.004

Chowdhury, M.S. (2024) Morphometric analysis of Halda River basin, Bangladesh, using GIS and remote sensing techniques. *Heliyon.*, 10(7), e29085. Available from: https://doi.org/10.1016/j.heliyon.2024.e29085

Christen, M., Kowalski, J. & Bartelt, P. (2010) RAMMS: numerical simulation of dense snow avalanches in three-dimensional terrain. *Cold Regions Science and Technology*, 63(1–2), 1–14. Available from: https://doi.org/10.1016/j.coldregions.2010.04.005

Corominas, J. (1996) The angle of reach as a mobility index for small and large landslides. *Canadian Geotechnical Journal*, 33(2), 260–271. Available from: https://doi.org/10.1139/t96-005

Dahlquist, M.P., West, A.J. & Li, G. (2018) Landslide-driven drainage divide migration. *Geology*, 46(5), 403–406. Available from: https://doi.org/10.1130/G39916.1

Dai, W., Qiu, R., Wang, B., Lu, W., Zheng, G., Amankwah, S.O.Y., et al. (2023) Enhancing UAV-SfM photogrammetry for terrain modeling

from the perspective of spatial structure of errors. *Remote Sensing*, 15(17), 4305. Available from: https://doi.org/10.3390/rs15174305

Dai, W., Zheng, G., Antoniazza, G., Zhao, F., Chen, K., Lu, W., et al. (2023) Improving UAV-SfM photogrammetry for modelling high-relief terrain: image collection strategies and ground control quantity. *Earth Surface Processes and Landforms*, 48(14), 2884–2899. Available from: https://doi.org/10.1002/esp.5665

Degetto, M., Gregoretti, C. & Bernard, M. (2015) Comparative analysis of the differences between using LiDAR and contour-based DEMs for hydrological modeling of runoff generating debris flows in the Dolomites. *Frontiers in Earth Science*, 3, 21. Available from: https://doi.org/10.3389/feart.2015.00021

Fan, L., Lehmann, P., McArdell, B. & Or, D. (2017) Linking rainfall-induced landslides with debris flows runout patterns towards catchment scale hazard assessment. *Geomorphology*, 280, 1–15. Available from: https://doi.org/10.1016/j.geomorph.2016.10.007

Frey, H., Huggel, C., Bühler, Y., Buis, D., Burga, M.D., Choquevilca, W., et al. (2016) A robust debris-flow and GLOF risk management strategy for a data-scarce catchment in Santa Teresa, Peru. *Landslides*, 13(6), 1493–1507. Available from: https://doi.org/10.1007/s10346-015-0669-z

Fusco, F., Zito, C., Guerriero, L., Calcaterra, D., De Vita, P., Longoni, L., et al. (2024) Integrated analysis of triggering and runout susceptibility to landslide-induced debris flows in Alpine catchments. *Italian Journal of Engineering Geology and Environment*, 1(Special Issue 1), 149–156.

Grieve, S.W., Hales, T.C., Parker, R.N., Mudd, S.M. & Clubb, F.J. (2018) Controls on zero-order basin morphology. *Journal of Geophysical Research: Earth Surface*, 123(12), 3269–3291. Available from: https://doi.org/10.1029/2017jf004453

GSI (2005) *Geology and mineral resources of Kerala*, 2nd edition, vol. 30. Kolkata: Miscellaneous Publication of Geological Survey of India. Publication of Geological Survey of India.

Guinau, M., Vilajosana, I. & Vilaplana, J.M. (2007) GIS-based debris flow source and runout susceptibility assessment from DEM data–a case study in NW Nicaragua. *Natural Hazards and Earth System Sciences*, 7(6), 703–716. Available from: https://doi.org/10.5194/nhess-7-703-2007

Hao, L., Rajaneesh, A., Van Westen, C., Sajinkumar, K.S., Martha, T.R., Jaiswal, P., et al. (2020) Constructing a complete landslide inventory dataset for the 2018 monsoon disaster in Kerala, India, for land use change analysis. *Earth System Science Data*, 12(4), 2899–2918.

Hao, L., van Westen, C., Rajaneesh, A., Sajinkumar, K.S., Martha, T.R. & Jaiswal, P. (2022) Evaluating the relation between land use changes and the 2018 landslide disaster in Kerala, India. *Catena*, 216, 106363. Available from: https://doi.org/10.1016/j.catena.2022.106363

Hungr, O. (1995) A model for the runout analysis of rapid flow slides, debris flows, and avalanches. *Canadian Geotechnical Journal*, 32(4), 610–623. Available from: https://doi.org/10.1139/t95-063

Hussin, H.Y., Quan Luna, B., Van Westen, C.J., Christen, M., Malet, J.P. & Van Asch, T.W. (2012) Parameterization of a numerical 2-D debris flow model with entrainment: a case study of the Faucon catchment, southern French Alps. *Natural Hazards and Earth System Sciences*, 12(10), 3075–3090. Available from: https://doi.org/10.5194/nhess-12-3075-2012

Jain, N., Martha, T.R., Khanna, K., Roy, P. & Kumar, K.V. (2021) Major landslides in Kerala, India, during 2018–2020 period: an analysis using rainfall data and debris flow model. *Landslides*, 18(11), 3629–3645. Available from: https://doi.org/10.1007/s10346-021-01746-x

Jain, N., Roy, P., Jalan, P., Martha, T.R. & Das, I.C. (2024) Irshalwadi landslide in Western Ghats of India: observations from precursory slope movement, rainfall and soil moisture. *Natural Hazards Research*, 4(4), 579–583. Available from: https://doi.org/10.1016/j.nhres.2024.01.004

James, M.R. & Robson, S. (2014) Mitigating systematic error in topographic models derived from UAV and ground-based image networks. *Earth Surface Processes and Landforms*, 39(10), 1413–1420. Available from: https://doi.org/10.1002/esp.3609

Jiao, W., Cheng, B., Zhu, W., Liu, W., He, G., Wang, W., et al. (2008) Accuracy analysis of remote sensing image rectification. In: Tong, Q., Gao, W., Guo, H. & Wang, J. (Eds.) *Proceedings of SPIE-Remote sensing of the environment: 16th National Symposium on remote sensing of China*, vol. 7123. Bellingham, WA: SPIE, pp. 62–68. Available from: https://doi.org/10.1117/12.815554

Kellndorfer, J., Walker, W., Pierce, L., Dobson, C., Fites, J.A., Hunsaker, C., et al. (2004) Vegetation height estimation from shuttle radar topography mission and national elevation datasets. *Remote Sensing of Environment*, 93(3), 339–358. Available from: https://doi.org/10.1016/j.rse.2004.07.017

Kern, A.N., Addison, P., Oommen, T., Salazar, S.E. & Coffman, R.A. (2017) Machine learning based predictive modeling of debris flow probability following wildfire in the intermountain Western United States. *Mathematical Geosciences*, 49(6), 717–735. Available from: https://doi.org/10.1007/s11004-017-9681-2

Koçyiğit, Ö. & Gürer, I. (2007) Effect of the Voellmy coefficients on determining run-out distance: a case study at Uzungöl, Turkey. *Gazi University Journal of Science*, 20(3), 79–85.

Konecny, G. (1979) Methods and possibilities for digital differential rectification. *Photogrammetric Engineering and Remote Sensing*, 45(6), 727–734.

Korup, O. & Clague, J.J. (2009) Natural hazards, extreme events, and mountain topography. *Quaternary Science Reviews*, 28(11–12), 977–990. Available from: https://doi.org/10.1016/j.quascirev.2009.02.021

Krishnapriya, V.K., Amrutha, A.S., Rajaneesh, A., Pradeep, G.S., Sankar, G., Nandakumar, D., et al. (2025) From disaster to conservation: Geoheritage potential of the 2024 Wayanad landslide, India. *Geoheritage*, 17(4), 1–16.

Krishnapriya, V.K., Rajaneesh, A., Pradeep, G.S., Amrutha, A.S., Sajinkumar, K.S., Ali, Y.P., et al. (2025) Wayanad landslide of 2024, India: interplay of geological and climatic factors. *Journal of the Geological Society of India*, 101(9), 1419–1424. Available from: https://doi.org/10.17491/jgsi/2025/174254

Krishnapriya, V.K., Rajaneesh, A., Sajinkumar, K.S., Oommen, T., Ali, Y.P., Vasu, N.N., et al. (2024) A rapid run-out assessment methodology for the 2024 Wayanad debris flow. *Nature Natural Hazards*, 1(1), 41. Available from: https://doi.org/10.1038/s44304-024-00044-5

Krušić, J., Abolmasov, B. & Samardžić-Petrović, M. (2019) Influence of DEM resolution on numerical modelling of debris flows in RAMMS-Selanac case study. In: Uljarević, M., Zekan, S. & Ibrahimović D. (Eds.) *Proceedings of the 4th regional symposium on the adriatic–Balkan region*. Tuzla, Bosnia and Herzegovina: Geotechnical Society of Bosnia and Herzegovina, pp. 23–25. Available from: https://doi.org/10.35123/ReSyLAB_2019_27

Kumar, S., Sharma, A. & Singh, K. (2024) A comprehensive review on debris flow landslide assessment using rapid mass movement simulation (RAMMS). *Geotechnical and Geological Engineering*, 42(7), 5447–5475. Available from: https://doi.org/10.1007/s10706-024-02887-1

Kuriakose, S.L., Sankar, G. & Muraleedharan, C. (2009) History of landslide susceptibility and a chorology of landslide-prone areas in the Western Ghats of Kerala, India. *Environmental Geology*, 57(7), 1553–1568. Available from: https://doi.org/10.1007/s00254-008-1431-9

Larsen, M.C. & Torres-Sánchez, A.J. (1998) The frequency and distribution of recent landslides in three montane tropical regions of Puerto Rico. *Geomorphology*, 24(4), 309–331. Available from: https://doi.org/10.1016/S0169-555X(98)00023-3

Lee, H. & Han, D. (2020) Rectification of bowl-shape deformation of tidal flat DEM derived from UAV imaging. *Sensors*, 20(6), 1602. Available from: https://doi.org/10.3390/s20061602

Longoni, L.A.U.R.A., Arosio, D., Scaioni, M., Papini, M., Zanzi, L., Roncella, R., et al. (2012) Surface and subsurface non-invasive investigations to improve the characterization of a fractured rock mass. *Journal of Geophysics and Engineering*, 9(5), 461–472. Available from: https://doi.org/10.1088/1742-2132/9/5/461

Martha, T.R., Roy, P., Khanna, K., Mrinalni, K. & Kumar, K.V. (2019) Landslides mapped using satellite data in the Western Ghats of India after

excess rainfall during august 2018. *Current Science*, 117(5), 804–812. Available from: https://doi.org/10.18520/cs/v117/i5/804-812

Mathew, M.M., Sreelash, K., Mathew, M., Arulbalaji, P. & Padmalal, D. (2021) Spatiotemporal variability of rainfall and its effect on hydrological regime in a tropical monsoon-dominated domain of Western Ghats, India. *Journal of Hydrology: Regional Studies*, 36, 100861.

Megha, V., Joshi, V., Kakde, N., Jaybhaye, A. & Dhoble, D. (2019) Flood mapping and analysis using sentinel application platform (SNAP)–a case study of Kerala. *International Journal of Research in Engineering Science and Management*, 2, 486–488.

Melo, R. & Zêzere, J.L. (2017) Modeling debris flow initiation and run-out in recently burned areas using data-driven methods. *Natural Hazards*, 88(3), 1373–1407. Available from: https://doi.org/10.1007/s11069-017-2921-4

Michalsen M. A. (2018) Effect of the DEMs resolution on landslide runout models (Master's thesis)

Mikoš, M. & Bezak, N. (2021) Debris flow modelling using RAMMS model in the Alpine environment with focus on the model parameters and Main characteristics. *Frontiers in Earth Science*, 8, 605061. Available from: https://doi.org/10.3389/feart.2020.605061

Mitchell, A., Zubrycky, S., McDougall, S., Aaron, J., Jacquemart, M., Hübl, J., et al. (2021) Variable hydrograph inputs for a numerical debris-flow runout model. *Natural Hazards and Earth System Sciences Discussions*, 2021, 1–44.

Mohamed, A.A.E. (2008) Development and application of digital elevation model rectification method in monitoring soil microtopography changes during rainfall. *Journal of Japan Society of Hydrology and Water Resources*, 21(2), 114–125.

Morell, K.D., Alessio, P., Dunne, T. & Keller, E. (2021) Sediment recruitment and redistribution in mountain channel networks by post-wildfire debris flows. *Geophysical Research Letters*, 48(24), e2021GL095549. Available from: https://doi.org/10.1029/2021GL095549

Nagarajan, R., Roy, A., Vinod Kumar, R., Mukherjee, A. & Khire, M.V. (2000) Landslide hazard susceptibility mapping based on terrain and climatic factors for tropical monsoon regions. *Bulletin of Engineering Geology and the Environment*, 58(4), 275–287. Available from: https://doi.org/10.1007/s100649900032

Naidu, S., Sajinkumar, K.S., Oommen, T., Anuja, V.J., Samuel, R.A. & Muraleedharan, C. (2018) Early warning system for shallow landslides using rainfall threshold and slope stability analysis. *Geoscience Frontiers*, 9(6), 1871–1882.

Ng, K.Y. (2006) Landslide locations and drainage network development: a case study of Hong Kong. *Geomorphology*, 76(1–2), 229–239. Available from: https://doi.org/10.1016/j.geomorph.2005.10.008

Novak, K. (1992) Rectification of digital imagery. *Photogrammetric Engineering and Remote Sensing*, 58, 339–339.

Ouédraogo, M.M., Degré, A., Debouche, C. & Lisein, J. (2014) The evaluation of unmanned aerial system-based photogrammetry and terrestrial laser scanning to generate DEMs of agricultural watersheds. *Geomorphology*, 214, 339–355. Available from: https://doi.org/10.1016/j.geomorph.2014.02.016

Pareek, T., Bhuyan, K., van Westen, C., Rajaneesh, A., Sajinkumar, K.S., Lobardo, L. et al. (2024) Analysing the posterior predictive capability and usability of landslide susceptibility maps: a case of Kerala, India. *Landslides*, 22, 655–670. Available from: https://doi.org/10.1007/s10346-024-02389-4

Parsa, P.S.A. & Zehra, K. (2023) Disaster Risk Reduction with Special Reference to 2018 Kerala Floods and Approaches to Reduce Flood Vulnerability at River Basin. In: *International handbook of disaster research*. Singapore: Springer Nature Singapore, pp. 903–925.

Radice, A., Giorgetti, E., Brambilla, D., Longoni, L. & Papini, M. (2016) On integrated sediment transport modelling for flash events in mountain environments. *Acta Geophysica*, 60(1), 191–213. Available from: https://doi.org/10.4408/IJEGE.2024-01.S-17

Rajaneesh, A., Krishnapriya, V.K., Nikhil-Nedumpallile-Vasu, van Westen, C., Oommen, T., Banks, V.J., et al. (2025) Predicting debris flow pathways using volume-based thresholds for effective risk assessment. *Nature Natural Hazards*, 2(1), 1. Available from: https://doi.org/10.1038/s44304-024-00055-2

Rickenmann, D. (1999) Empirical relationships for debris flows. *Natural Hazards*, 19(1), 47–77. Available from: https://doi.org/10.1023/A:1008064220727

Rickenmann, D. & Koschni, A. (2010) Sediment loads due to fluvial transport and debris flows during the 2005 flood events in Switzerland. *Hydrological Processes*, 24(8), 993–1007. Available from: https://doi.org/10.1002/hyp.7536

Rickenmann, D., Laigle, D.M.B.W., McArdell, B.W. & Hübl, J. (2006) Comparison of 2D debris-flow simulation models with field events. *Computational Geosciences*, 10(2), 241–264. Available from: https://doi.org/10.1007/s10596-005-9021-3

Roncella, R. & Forlani, G. (2005) Extraction of planar patches from point clouds to retrieve dip and dip direction of rock discontinuities. In: Vosselman, G. & Brenner, C. (Eds.) *Proceedings of the ISPRS workshop laser scanning*, vol. 36. no. 3/W19. Enschede, The Netherlands: International Society for Photogrammetry and Remote Sensing (ISPRS), pp. 162–167.

Sajinkumar, K.S. & Anbazhagan, S. (2015) Geomorphic appraisal of landslides on the windward slope of Western Ghats, southern India. *Natural Hazards*, 75(1), 953–973. Available from: https://doi.org/10.1007/s11069-014-1358-2

Sajinkumar, K.S., Arya, A., Rajaneesh, A., Oommen, T., Yunus, A.P., Rani, V.R., et al. (2022) Migrating rivers, consequent paleochannels: the unlikely partners and hotspots of flooding. *Science of the Total Environment*, 807(Pt 2), 150842. Available from: https://doi.org/10.1016/j.scitotenv.2021.150842

Sajinkumar, K.S. & Oommen, T. (2020) Rajamala landslide: continuation of a never-ending landslide series. *Geological Society of India*, 96(3), 310.

Sajinkumar, K.S. & Oommen, T. (2021) *Landslide atlas of Kerala*, vol. 7, no. 1. Bengaluru: GSI Publications.

Saleem, N., Huq, M.E., Twumasi, N.Y.D., Javed, A. & Sajjad, A. (2019) Parameters derived from and/or used with digital elevation models (DEMs) for landslide susceptibility mapping and landslide risk assessment: a review. *ISPRS International Journal of Geo-Information*, 8(12), 545. Available from: https://doi.org/10.3390/ijgi8120545

Salm, B. (1993) Flow, flow transition and runout distances of flowing avalanches. *Annals of Glaciology*, 18, 221–226. Available from: https://doi.org/10.3189/S0260305500011551

Sankar, G. (2018) Monsoon Fury in Kerala—a geo-environmental appraisal. *Journal of the Geological Society of India*, 92(4), 383–388. Available from: https://doi.org/10.1007/s12594-018-1031-6

dos Santos Corrêa, C.V., Reis, F.A.G.V., do Carmo Giordano, L., Cabral, V.C., Veloso, V.Q. & D'Affonseca, F.M. (2024) Numerical modeling of a high magnitude debris-flow event occurred in Brazil. *Natural Hazards*, 120(14), 13077–13107. Available from: https://doi.org/10.1007/s11069-024-06728-5

Sharma, U., Ray, Y. & Pandey, M. (2022) Topography and rainfall coupled landscape evolution of the passive margin of Sahyadri (Western Ghats), India. *Geosystems and Geoenvironment*, 1(4), 100100.

Sim, K.B., Lee, M.L. & Wong, S.Y. (2022) A review of landslide acceptable risk and tolerable risk. *Geoenvironmental Disasters*, 9(1), 3. Available from: https://doi.org/10.1186/s40677-022-00205-6

Svalova, V.B., Zaalishvili, V.B., Ganapathy, G.P., Nikolaev, A.V. & Melkov, D.A. (2019) Landslide risk in mountain areas. *Geology and Geophysics of the South of Russia*, 9(2), 110–123. Available from: https://doi.org/10.23671/VNC.2019.2.31981

Thampi, P.K. (1997) *Evaluation study in terms of landslide mitigation in parts of western Ghats Kerala, India*. Trivandrum: Centre for Earth Science Studies.

Tucker, G.E. & Hancock, G.R. (2010) Modelling landscape evolution. *Earth Surface Processes and Landforms*, 35(1), 28–50. Available from: https://doi.org/10.1002/esp.1952

Tuominen, S., Balazs, A., Saari, H., Pölönen, I., Sarkeala, J. & Viitala, R. (2015) Unmanned aerial system imagery and photogrammetric canopy height data in area-based estimation of forest variables. *Silva Fennica*, 49(5), 1348. Available from: https://doi.org/10.14214/sf.1348

Veloso, V.Q., Reis, F.A.V.G., Cabral, V., Zaine, J.E., dos Santos Corrêa, C.V., Gramani, M.F., et al. (2023) Hazard assessment of debris-flow-prone watersheds in Cubatão, São Paulo state, Brazil. *Natural Hazards*,

116(3), 3119–3138. Available from: https://doi.org/10.1007/s11069-022-05800-2

Vishnu, C.L., Oommen, T., Chatterjee, S. & Sajinkumar, K.S. (2022) Challenges of modeling rainfall triggered landslides in a data-sparse region: a case study from the Western Ghats, India. *Geosystems and Geoenvironment*, 1(3), 100060. Available from: https://doi.org/10.1016/j.geogeo.2022.100060

Vishnu, C.L., Rani, V.R., Sajinkumar, K.S., Oommen, T., Bonali, F.L., Pareeth, S., et al. (2020) Catastrophic flood of august 2018, Kerala, India: study of partitioning role of lineaments in modulating flood level using remote sensing data. *Remote Sensing Applications: Society and Environment*, 20, 100426. Available from: https://doi.org/10.1016/j.rsase.2020.100426

Vishnu, C.L., Sajinkumar, K.S., Oommen, T., Coffman, R.A., Thrivikramji, K.P., Rani, V.R., et al. (2019) Satellite-based assessment of the august 2018 flood in parts of Kerala, India. *Geomatics, Natural Hazards and Risk*, 10(1), 758–767. Available from: https://doi.org/10.1080/19475705.2018.1543212

Voellmy, A. (1955) Uber die zerstorungskraft von lawinen. *Bauzeitung*, 73, 159–165.

Wackrow, R. & Chandler, J.H. (2011) Minimising systematic error surfaces in digital elevation models using oblique convergent imagery. *The Photogrammetric Record*, 26(133), 16–31. Available from: https://doi.org/10.1111/j.1477-9730.2011.00623.x

Wang, Q., Fang, N., Zeng, Y., Yuan, C., Dai, W., Fan, R., et al. (2025) Optimizing UAV-SfM photogrammetry for efficient monitoring of gully erosion in high-relief terrains. *Measurement*, 256(Part A), 118154. Available from: https://doi.org/10.1016/j.measurement.2025.118154

WSL Institute for SnowAvalanche Research SLF (2022). *RAMMS:: DEBRISFLOW user manual a numerical model for debris flows in research and practice user manual v1.8.0 debris flow RAMMS rapid mass movement simulation*. Davos Dorf, Switzerland: WSL Institute for Snow and Avalanche Research SLF. Available at: https://ramms.slf.ch/ramms/downloads/RAMMS_DBF_Manual.pdf

Xia, W., Chen, J., Liu, J., Ma, C. & Liu, W. (2021) Landslide extraction from high-resolution remote sensing imagery using fully convolutional spectral–topographic fusion network. *Remote Sensing*, 13(24), 5116. Available from: https://doi.org/10.3390/rs13245116

Yang, H., Yang, T., Zhang, S., Zhao, F., Hu, K. & Jiang, Y. (2020) Rainfall-induced landslides and debris flow in Mengdong town, Yunnan Province, China. *Landslides*, 17, 931–941.

Yesubabu, V., Thomas, B., Srinivas, C.V., Basha, G. & Kunchala, R.K. (2024) Impact of Western Ghats orography on the simulation of extreme precipitation over Kerala, India during 14–17 august 2018. *Atmospheric Research*, 299, 107211. Available from: https://doi.org/10.1016/j.atmosres.2023.107211

Yunus, A.P., Fan, X., Subramanian, S.S., Jie, D. & Xu, Q. (2021) Unraveling the drivers of intensified landslide regimes in Western Ghats, India. *Science of the Total Environment*, 770, 145357. Available from: https://doi.org/10.1016/j.scitotenv.2021.145357

Yunus, A.P., Ishan, A., Magesh, N.S., Sajinkumar, K.S., Scaringi, G., Subramanian, S.S., et al. (2025) Rapid evacuation of suspended sediment loads during landslides in steep gradient rivers. *Environmental Research Communications*, 7(3), 031002. Available from: https://doi.org/10.1088/2515-7620/adb8a7

Yunus, A.P., Sajinkumar, K.S., Gopinath, G., Subramanian, S.S., Kaushal, S., Thanveer, J., et al. (2025) Chronicle of destruction: the Wayanad landslide of July 30, 2024. *Landslides*, 22(6), 1–1908. Available from: https://doi.org/10.1007/s10346-025-02494-y

Zhang, Y.X. (2019) Numerical simulation of debris flow runout using Ramms: a case study of Luzhuang gully in China. *Computer Modeling in Engineering and Sciences*, 121(3), 981–1009. Available from: https://doi.org/10.32604/cmes.2019.07337

Zhao, S., Wang, L., Cheng, W., Liu, H. & He, W. (2015) Rectification methods comparison for the ASTER GDEM V2 data using the ICESat/GLA14 data in the Lvliang mountains, China. *Environmental Earth Sciences*, 74(8), 6571–6590. Available from: https://doi.org/10.1007/s12665-015-4614-1

SUPPORTING INFORMATION

Additional supporting information can be found online in the Supporting Information section at the end of this article.

How to cite this article: V. K., K., A., R., K. S., S., Nedumpallile-Vasu, N., Ali, Y.P., Hao, L. et al. (2026) High-resolution LiDAR and stereo-DEMs for debris flow analysis in the Western Ghats, India: Sediment volume computation and run-out modeling. *Earth Surface Processes and Landforms*, 51(3), e70272. Available from: https://doi.org/10.1002/esp.70272